CHALMERS
FINITE ELEMENT CENTER

PREPRINT 2001–08

Adaptive finite element computation of 3D magnetostatic problems in potential formulation

Marzia Fontana

Chalmers Finite Element Center
CHALMERS UNIVERSITY OF TECHNOLOGY
Göteborg Sweden 2001

CHALMERS FINITE ELEMENT CENTER

Preprint 2001–08

Adaptive finite element computation of 3D magnetostatic problems in potential formulation

Marzia Fontana

CHALMERS

Chalmers Finite Element Center
Chalmers University of Technology
SE–412 96 Göteborg Sweden
Göteborg, April 2001

Adaptive finite element computation of 3D magnetostatic problems in potential formulation
Marzia Fontana
NO 2001–08
ISSN 1404–4382

Chalmers Finite Element Center
Chalmers University of Technology
SE–412 96 Göteborg
Sweden
Telephone: +46 (0)31 772 1000
Fax: +46 (0)31 772 3595
www.phi.chalmers.se

Printed in Sweden
Chalmers University of Technology
Göteborg, Sweden 2001

Adaptive finite element computation of 3D magnetostatic problems in potential formulation

MARZIA FONTANA [1]

Abstract

A finite element analysis is proposed for the static 3D Maxwell's equations for magnetic fields, based on a double potential formulation that leads to a generalized Poisson model with discontinuous diffusion and non-homogeneous Dirichlet and Neumann interface and boundary conditions. The finite element method consists of a piecewise linear Galerkin discretization on a tetrahedral mesh. In the modelling phase, the computation of the Biot-Savart law is performed by finite volume integration in case of complex-shaped current-carrying geometries, or mixed semi-numerical and analytical Urankar's formulas in case of coil geometries. An adaptive criterion of mesh refinement is then applied, based on a posteriori estimation of the finite element error in energy norm. Numerical examples on some magnetostatic cases are presented for a comparison with other adaptive finite element techniques.

Key words - Finite element methods, a posteriori error, adaptive mesh refinement, magnetostatic problems, Biot-Savart law.

[1]E-mail address: *marzia@math.chalmers.se*, *marzia@iname.com*
Chalmers Finite Element Center, Department of Mathematics, Chalmers University of Technology
S-41296 Göteborg, Sweden.
Work supported by CNR research fellowship 203.01.70, Consiglio Nazionale delle Ricerche, Italy
2000 Mathematics Subject Classification: 35J25, 65N30, 65N50, 78A30

Contents

Thus the partial differential equation
entered theoretical physics as a handmaid,
but has gradually become mistress.
(A. Einstein, *"The World as I See It"*)

1 Introduction

Mathematical modelling plays an essential role in science and engineering. In most cases, for a deep understanding of physical phenomena and to find answers to engineering problems, it is necessary to go beyond experiments and heuristic methods and rather follow a theoretical approach from above, through a formal representation in terms of a *mathematical model*. Many problems can be modelled by systems of functional equations with given boundary and/or initial conditions. In most cases, such functional equations are partial or ordinary differential equations, so that evolution models are represented by initial boundary value problems and stationary models by boundary value problems, both linear and non-linear [19]. Only pure differential modelling is not, however, sufficient to explain the complexity of all physical behaviours: in some fields of physics and engineering, in fact, phenomena and properties need to be formulated by difference, integral or integro-differential equations. Once the mathematical model has been formulated in such a way that it has a solution, the interest is then to solve it. Since very seldom an analytical solution is obtainable, numerical methods take over analytical ones from giving approximate, *computable* solutions. The analysis is carried out passing through the following basic stages: (1) *real problem*, (2) *mathematical model*, (3) *discrete model*, (4) *numerical solution*. The computed solution is thus the approximation of the investigated physical properties in the real problem under consideration.

We here point out the term *approximation*: no equations describe physical reality exactly, namely the computed solution is subject to *error*. What we call error is actually the sum of several independent contributions due to the several phases of modelling, discretization and computation. Regarding this, an interesting development in Computational Mathematics is to measure the several contributions of the error, in order to estimate the accuracy of the numerical solution and suggest criteria to improve it. Later on we will turn back to this important aspect.

In this general outline of mathematical modelling, we here focus on *electromagnetic models* [16, 28]. A vast amount of problems and devices around us are explained by electromagnetic theories: cathode-ray oscilloscopes, television reception, radar, satellite communication, microwave devices, mobile communication, optical fiber communication, remote sensing, radio astronomy, brain scanners, electromagnetic shielding, particle accelerators, MRI systems, electromagnetic compatibility aspects, problems of electro-mechanical energy conversion, and so on. As known, the fundamental equations in physics governing all macroscopic electromagnetic phenomena are *Maxwell's equations*, expressed by an hyperbolic system of first order differential equations. The main task of mathematical modelling in electromagnetic analysis is then the problem of solving Maxwell's equations under given boundary and initial conditions. Analytical solutions of Maxwell's equations do exist in fact, obtained mainly by separation of variables and Fourier and Laplace transform methods, but they are based on simple coordinate systems with regular or infinite boundaries. Such analytical methods require too strict assumptions on the geometry of the material regions and, somehow, too ideal hypotheses that cannot match the complex shapes of electromagnetic devices and domains encountered in real life and industrial applications. We realize, therefore, the importance of numerical tools since analytical methods do not exist in most of the cases of interest.

As it happens in other engineering fields, various numerical methods can be used to solve differential models in electromagnetism. Typically, *finite element*, *finite difference*, *spectral* and *boundary element methods* are used, or mixed approached based on a combination of these techniques [37]. Evidently, both theoretical and practical reasons arise in the choice of the appropriate numerical technique, depending on the nature of the problem (e.g. the domain geometry, possible a priori known properties of the solution, and so on), but also on the available resources in terms of time and means. Sometimes, still now, constraints of low computational time and cost can force to use simpler discretization schemes at low order (e.g. finite difference methods). Nevertheless, problems on complex-shaped devices, or requiring high precision, address towards more robust and accurate numerical methods. Among them, the finite element method (FEM) has recently become a standard computation technique [30, 50].

The first finite element methods were introduced by R. Courant in 1943, developed in the successive years for structural analysis applications in aircraft design (elasticity equations, plate equations, etc.). A solid mathematical background was developed in the 1960s for elliptic problems, then extended to parabolic and hyperbolic problems later. From then on, with the coming of automatic computation, this method has had a wide diffusion in many engineering applications: structural and solid state mechanics, fluid dynamics, nuclear engineering, heat conduction, convection-diffusion processes, petroleum engineering, reaction-diffusion processes, electromagnetism, wave propagation, integration circuits, and so on. Concerning electromagnetic models, finite element methods are currently utilized for a vast amount of static, quasi-static and time dependent problems, ranging from high frequency microwaves used in mobile communication to low frequency occurring in power energy [29, 34, 42, 45].

Basically, two different approaches can be used: *nodal* finite elements, typical of scalar formulations, as well as *edge* finite elements. The former have been mainly used until now. The latter [29] were introduced by H. Whitney in the 1950s, but only in recent years some edge finite element theories (J.C. Nedelec, A. Bossavit, and others) have received an increasing attention for vector formulations. An advantage of edge elements in a vector formulation of electromagnetic problems is that they can model discontinuities of the field variables in the transition across different material domains, with abrupt changes in electric conductivity, permittivity or magnetic permeability. The nodal approach, however, is still preferred for scalar potential formulations (as in our case).

Concerning the shape of elements used in space discretization, most of the earlier finite element literature had been developed for rectangles in two dimensions and bricks in three dimensions. Especially for electromagnetic applications, however, there has been recently an increasing interest towards triangular and tetrahedral meshes, as they handle better corners and edges occurring in the complex shapes of electromagnetic devices.

Furthermore, an area of increasing interest is given by *adaptive* finite element methods [3, 5, 7, 18, 32, 33, 49]. Differently from classical techniques, in adaptive methods an improvement of the solution accuracy is reached by a local refinement of the mesh, or a local increase of the polynomial order of the finite element solution, performed only on a selection on mesh elements having large error indicators. Such indicators are computed by suitable *a posteriori* error estimates of the finite element solution obtained according to different criteria, and measured by known quantities, like the numerical solution, the data and the mesh size. An adaptive approach allows to reduce in a significant way the computational cost and time of the finite element calculation on the model.

Following these guidelines, the purpose of this work is to study the efficiency of adaptive finite element methods on some three-dimensional magnetostatic problems obtained from a double potential formulation of static Maxwell's equations, with a posteriori error estimation. The idea is carried out through an analysis at more levels, which involve both modelling and computation aspects. Concerning the modelling phase, a significant and crucial task is the integration of the Biot-Savart law for the estimation of the magnetic field due to source currents.

The report is organized as follows.

In Chapter 2 the mathematical background is presented, with a short overview of Lebesgue and Sobolev spaces used in the variational formulation and finite element analysis of the magnetostatic models studied in the present work.

Chapter 3 presents an introductory scenario on fundamental mathematical models used in electromagnetic problems, derived from Maxwell's equations. Two different mathematical modelling approaches are discussed: *field* formulations, based on vector fields $\mathbf{E}$, $\mathbf{D}$, $\mathbf{H}$ and $\mathbf{B}$, or *potential* formulations, introducing scalar and vector potentials, like V, $\mathbf{A}$, $\mathbf{T}$, χ, and the combination ϕ-φ (considered in the present work).

Chapter 4 describes the general class of boundary value problems to which magnetostatic models in φ-ϕ potential formulation belong. The abstract model is an elliptic problem, consisting of a generalized Poisson equation with mixed non-homogeneous boundary and interface conditions of Dirichlet and Neumann type. The variational formulation is then discussed, and existence and uniqueness of the weak solution is proved by the Lax-Milgram theorem, with successive finite element discretization by Galerkin method on tetrahedral mesh.

A formal error analysis is then presented in Chapter 5. Modelling and computational errors are discussed and, focusing on the computational error due to the finite element discretization, a priori and a posteriori approaches are explained. A posteriori error estimates are then proved in energy norm, as quantitative indicators of accuracy of the finite element solution. Geometric techniques of element subdivision for an adaptive refinement of the mesh, based on these error indicators, are then discussed.

Aspects about implementation are investigated in Chapter 6. A general description of the algorithm is first provided. The successive sections are then dedicated to explain possible advantages of object-oriented programming for finite element computations with some examples of finite element classes, as they have been used in the implementation of our algorithm.

Finally, numerical results are reported in Chapter 7. Two test cases are proposed, based on convex and non-convex geometries, involving magnetic soft materials with different magnetic permeabilities. Results are discussed for a comparison with the ones already obtained by finite element methods for the static Maxwell's equations in field formulation, e.g the least-squares finite element method, a dual formulation known as $\mathcal{L}\mathcal{L}^*$ method, and a vector potential formulation by using nodal or edge elements. These methods have been tested at Chalmers Finite Element Center, an interdisciplinary unit of Chalmers University of Technology in Göteborg, Sweden, in cooperation with ABB Corporate Research.

2 Mathematical background

In this section we introduce notations and definitions about Lebesgue and Sobolev spaces with a short mention to some basic properties and inequalities used in the following.

Notation. Throughout this document, the symbols $\mathbb{C}$, $\mathbb{R}$ and $\mathbb{N}$ denote the set of complex, real and natural (0 included) numbers, respectively. C is reserved for a real positive constant, different at each occurrence. For any domain Ω in the Euclidean space $\mathbb{R}^n$, notations $\partial\Omega$, $\overline{\Omega}$ and $\dot{\Omega}$ denote the boundary, the closure and the interior part of Ω, respectively.

2.1 Lebesgue spaces

Let Ω be an open Lebesgue measurable domain in $\mathbb{R}^n$. If Ω is bounded, we assume that its boundary $\partial\Omega$ is "sufficiently" regular, i.e. Lipschitz continuous. For any real $p \geq 1$, we denote by $L_p(\Omega)$ the *Lebesgue space of order* p, i.e. the Banach space of all equivalence classes of real or complex-valued functions u Lebesgue integrable on Ω, in which the p-powers of $|\, u\,|$ are Lebesgue integrable on Ω. Denoting by $d\mathbf{x} = dx_1 dx_2 \dots dx_n$, the standard norm in $L_p(\Omega)$ is defined as

$$\|\, u\,\|_{L_p(\Omega)} = \Big(\int_\Omega |\, u\,|^p d\mathbf{x} \Big)^{1/p}, \quad \forall u \in L_p(\Omega). \tag{2.1}$$

Functions in L_p are not continuous in general but, broadly speaking, they are a sort of "weak" approximation of continuous functions. This follows from the fact that the set $C(\overline{\Omega})$ is dense in $L_p(\Omega)$.

Among the Lebesgue spaces, it is known that $L_2(\Omega)$ is an Hilbert space, by choosing the inner product

$$(u, v)_{L_2(\Omega)} = \int_\Omega u\, \overline{v}\, d\mathbf{x}, \quad \forall u, v \in L_2(\Omega), \tag{2.2}$$

whose induced norm coincides with the Lebesgue norm (2.1) for $p = 2$. In case of real-valued functions, definition (2.2) and similar ones are given by setting v in place of the conjugate $\overline{v}$. The well-known *Cauchy-Schwartz inequality* holds, that is

$$|\,(u, v)_{L_2(\Omega)}\,| \leq \|\, u\,\|_{L_2(\Omega)} \|\, v\,\|_{L_2(\Omega)}, \quad \forall u, v \in L_2(\Omega). \tag{2.3}$$

Relation (2.3) can be seen as a particular case, for $p = q = 2$, of *Hölder's inequality*, which asserts that for all $p \geq 1$, $q \geq 1$ such that $1/p + 1/q = 1$, if $u \in L_p(\Omega), v \in L_q(\Omega)$, then $u\, v \in L_1(\Omega)$ and

$$\|\, u\, v\,\|_{L_1(\Omega)} \leq \|\, u\,\|_{L_p(\Omega)} \|\, v\,\|_{L_q(\Omega)}. \tag{2.4}$$

We also introduce $L_\infty(\Omega)$ as the Banach space of all equivalence classes of real or complex-valued functions u Lebesgue integrable on Ω, essentially (i.e. *almost everywhere*) bounded on Ω. The corresponding norm is defined as

$$\| u \|_{L_\infty(\Omega)} = ess\ \sup_\Omega | u |= \inf\{M \in \mathbb{R} : | u(\mathbf{x}) |\leq M \text{ a.e. in } \Omega\}. \tag{2.5}$$

Notice that the notation $L_\infty(\Omega)$ is justified by a limit property: for a given function u Lebesgue integrable on Ω, if a real $q \geq 1$ exists such that $\| u \|_{L_q(\Omega)} < +\infty$ then $\| u \|_{L_p(\Omega)} \rightarrow \| u \|_{L_\infty(\Omega)}$ as $p \to \infty$. The inclusion $L_q(\Omega) \subseteq L_p(\Omega)$ for $1 \leq p \leq q$ holds, from Hölder's inequality, as well as $L_p(\Omega) \subseteq L_\infty(\Omega)$ for any $p \geq 1$. Moreover, there exists a constant $C > 0$ such that

$$\| u \|_{L_p(\Omega)} \leq C \| u \|_{L_q(\Omega)}, \quad \forall u \in L_q(\Omega). \tag{2.6}$$

For a more extended survey of Lebesgue spaces, see [40].

2.2 Sobolev spaces

A finite element analysis requires a further assumption of regularity on L_2-functions. Regarding this, for each $m \in \mathbb{N}$, we define the *Sobolev spaces of order* m as

$$H^m(\Omega) = \{u \in L_2(\Omega) : \ D^\alpha u \in L_2(\Omega), \ \forall \alpha : | \alpha |\leq m\} \tag{2.7}$$

for any multi-index $\alpha = (\alpha_1, \alpha_2, \dots \alpha_n) \in \mathbb{N}^n$ with $| \alpha |= \sum_{i=1}^n \alpha_i$, where the derivatives

$$D^\alpha u = \frac{\partial^{|\alpha|} u}{\partial^{\alpha_1} x_1 \, \partial^{\alpha_2} x_2 \dots \partial^{\alpha_n} x_n} \tag{2.8}$$

are intended in the sense of *distributions* [22]. $H^m(\Omega)$ is an Hilbert space with the inner product

$$(u, v)_{H^m(\Omega)} = \sum_{|\alpha| \leq m} \int_\Omega D^\alpha u \, D^\alpha \overline{v} \; d\mathbf{x}, \quad \forall u, v \in H^m(\Omega), \tag{2.9}$$

whose induced norm is

$$\| u \|_{H^m(\Omega)} = \Big(\sum_{|\alpha| \leq m} \| D^\alpha u \|^2_{L_2(\Omega)} \Big)^{1/2}, \quad \forall u \in H^m(\Omega). \tag{2.10}$$

Further, an important seminorm is defined as

$$| u |_{H^m(\Omega)} = \Big(\sum_{|\alpha|=m} \| D^\alpha u \|^2_{L_2(\Omega)} \Big)^{1/2}, \quad \forall u \in H^m(\Omega). \tag{2.11}$$

Immediately we have $H^m(\Omega) \subseteq H^{m-1}(\Omega)$ for $m = 1, 2, \ldots$, with

$$\| u \|_{H^{m-1}(\Omega)} \leq \| u \|_{H^m(\Omega)}, \quad \forall u \in H^m(\Omega). \tag{2.12}$$

Concerning continuity properties, we first denote by $C_b^m(\overline{\Omega})$ the space of real or complex-valued functions on $\overline{\Omega}$ whose classical derivatives up to order m are continuous and bounded. This is a Banach space, equipped with the norm

$$\| u \|_{C_b^m(\overline{\Omega})} = \sum_{|\alpha| \leq m} \sup_{\mathbf{x} \in \overline{\Omega}} | D^\alpha u(\mathbf{x}) |, \quad \forall u \in C_b^m(\overline{\Omega}). \tag{2.13}$$

Then, inclusion $C_b^m(\overline{\Omega}) \subseteq H^m(\Omega)$ holds for all $m = 0, 1, 2, \ldots$. On the other hand, functions in $H^m(\Omega)$ are not continuous in general. By the so-called *Sobolev embedding theorem* it is possible to prove, nevertheless, that "good" properties of regularity are satisfied when m is sufficiently high. In particular, in one dimension all H^1-functions are continuous; in two and three dimensions H^2-functions are continuous, while H^1-functions are not in general. Precisely, if $m > n/2$ then $H^m(\Omega) \subseteq C_b^0(\overline{\Omega})$ and there exists a constant $C > 0$ such that

$$\| u \|_{C_b^0(\overline{\Omega})} \leq C \| u \|_{H^m(\Omega)}, \quad \forall u \in H^m(\Omega). \tag{2.14}$$

More generally, if $k \in \mathbf{N}$ and $m > n/2 + k$ then there exists a constant $C > 0$ such that

$$\| D^\alpha u \|_{L_\infty(\Omega)} \leq C \| u \|_{H^m(\Omega)}, \quad \forall u \in H^m(\Omega), \tag{2.15}$$

for all $\alpha \in \mathbf{N}^n$ such that $|\alpha| \leq k$.

For a finite element formulation of second order boundary value problems, as in our case, a "weak" regularity on the first derivative of the functions is required by applying Green's theorem [37]. Thus, $H^1(\Omega)$ turns out to be the fundamental setting for our problems.

Suppose now that the domain Ω is bounded. Differently from L_2-functions, for any $\Gamma \subseteq \partial\Omega$ the restriction $\gamma u = u|_\Gamma$ of a function $u \in H^1(\Omega)$ is well-defined, in the sense intended by the well-known *trace theorem* [22]. The function γu belongs to $L_2(\Gamma)$ and is called the *trace* of u on Γ. Regarding this, the most classical *trace inequality* asserts that there exists a constant $C > 0$ depending only on Ω such that

$$\| \gamma u \|_{L_2(\Gamma)} \leq C \| u \|_{H^1(\Omega)}, \quad \forall u \in H^1(\Omega), \tag{2.16}$$

where the definition of the spaces $L_p(\Gamma)$ with corresponding norms $\|\cdot\|_{L_p(\Gamma)}$ is given analogously to (2.1), using Γ as integration domain.

We denote by $\mathcal{D}(\Omega)$ the space of infinitely differentiable functions with compact support in Ω, i.e. assuming non-zero values only on some compact subset of Ω. An important subspace in $H^1(\Omega)$ is then $H^1_0(\Omega)$, which is defined as the closure of $\mathcal{D}(\Omega)$ in $H^1(\Omega)$. It can be shown that

$$H^1_0(\Omega) = \{u \in H^1(\Omega) :\ u|_{\partial\Omega} = 0\}. \tag{2.17}$$

$H^1_0(\Omega)$ turns out to be the natural space associated to finite element solutions of second order boundary value problems with boundary conditions all of Dirichlet type. Coherently, the space

$$H^1_{0,\Gamma}(\Omega) = \{u \in H^1(\Omega) :\ u|_{\Gamma} = 0\} \tag{2.18}$$

can be introduced for $\Gamma \subseteq \partial\Omega$, as a natural setting when both Dirichlet and Neumann (or Robin) boundary conditions are present, the former given on Γ. Note that in $H^1_0(\Omega)$ the seminorm $\|u\|^*_{H^1_0(\Omega)} = \|\nabla u\|_{L_2(\Omega)}$, obtained from (2.11) for $m = 1$, is a norm equivalent to the Sobolev norm (2.10) (and analogously for $H^1_{0,\Gamma}(\Omega)$). Norms $\|\cdot\|^*_{H^1_0(\Omega)}$ and $\|\cdot\|_{L_2}$ are related to each other through the following *Poincaré's inequality*: if Ω is bounded, there exists a constant $C > 0$ depending on Ω such that

$$\|u\|_{L_2(\Omega)} \le C\|\nabla u\|_{L_2(\Omega)}, \quad \forall u \in H^1_0(\Omega). \tag{2.19}$$

Immediately, an inequality analogous to (2.19) holds again when considering at the left hand side $\|u\|_{H^1(\Omega)}$ instead of $\|u\|_{L_2(\Omega)}$.

In boundary value problems functions have to be assigned as data over parts of domain boundaries. Thus, it makes sense to introduce the space

$$H^{1/2}(\Gamma) = \{v\colon \Gamma \to \mathbb{R}\ (\text{or } \mathbb{C}) :\ \exists u \in H^1(\Omega) :\ u\,|_\Gamma = v\}, \tag{2.20}$$

belonging to a more general family of Sobolev spaces $H^r(\Omega)$ for $r \in \mathbb{R}$, which can be defined by Fourier transform [22], consistently with definition (2.7) when $r = m \in \mathbb{N}$. $H^{1/2}(\Gamma)$ is an Hilbert space, endowed with the norm

$$\|v\|_{H^{1/2}(\Gamma)} = \inf_{\substack{u \in H^1(\Omega) \\ u|_\Gamma = v}} \|u\|_{H^1(\Omega)}, \quad \forall v \in H^{1/2}(\Gamma). \tag{2.21}$$

When working with spaces $H^r(\Omega)$ having real order r, an useful inequality is given by the following *interpolation theorem*: if Ω is bounded and $r_1,\ r_2$ are real numbers such that $r_1 < r_2$, then there exists a constant $C > 0$ such that

$$\| u \|_{H^r(\Omega)} \leq C \| u \|_{H^{r_1}(\Omega)}^{1-\theta} \| u \|_{H^{r_2}(\Omega)}^{\theta}, \quad \forall v \in H^{r_2}(\Omega) \tag{2.22}$$

where $r = (1-\theta)r_1 + \theta\, r_2$, for any $0 \leq \theta \leq 1$.

Further generalizations can be done. First, similarly to definition (2.7), *generalized Sobolev spaces of order* m, denoted by $W^{m,p}(\Omega)$, can be introduced in connection with spaces $L_p(\Omega)$. $W^{m,p}(\Omega)$ are Banach spaces in which elements are L_p-functions whose derivatives up to order m are L_p-functions, so that $H^m(\Omega) = W^{m,2}(\Omega)$.

Still considering the case $p = 2$, when differential models involve not scalar but vector functions having d components, spaces $H^m(\Omega; \mathbb{R}^d)$ or $H^m(\Omega; \mathbb{C}^d)$ can be naturally introduced to describe a H^m-regularity for each component. Besides, for vector differential equations using divergence of curl operators, spaces like $H(div; \Omega)$, or $H(curl; \Omega)$ can be used, requiring a L_2-regularity on the divergence or the curl of the functions, respectively. In the framework of electromagnetic models, for instance, the last two turn out to be suitable settings for the finite element solution of problems defined by Maxwell's equations when a field formulation is used (see Chapter 3).

Furthermore, functional spaces for time dependent functions could be introduced as natural settings for finite element methods solving initial boundary value problems. Let $[0, T]$ be the time interval and let $V(\Omega)$ denote a suitable Banach or Hilbert space of functions defined almost everywhere on Ω and sufficiently regular (in a weak sense). Then, it can be convenient to introduce spaces like $C^0([0, T]; V(\Omega))$, requiring continuity on variable t, or "weaker" spaces like the *time dependent Lebesgue space* $L_2(0, T; V(\Omega))$ and the *time dependent Sobolev space* $H^1(0, T; V(\Omega))$, and analogously $H^m(0, T; V(\Omega))$. The space $V(\Omega)$ can be, for instance, $L_2(\Omega)$ or $H^1(\Omega)$.

In [22, 38] a detailed analysis on Sobolev spaces and their generalizations is presented, together with an extended survey of mathematical topics related to partial differential equations. A general overview of several methods for the numerical solution of differential problems can be found in [37]. Finite element methods on a large class of problems are presented in [30]. As concerns finite element methods for elliptic problems, considered in the present work, a classical reference is [17]. In particular, finite element modelling focusing on electromagnetic problems is presented in [29, 42, 45] and, from a rigorous mathematical point of view, in [34].

3 Field and potential equations in electromagnetism

3.1 Maxwell's equations

The fundamental equations describing electromagnetic phenomena are the well-known *Maxwell's equations.* For all space points, in the general time dependent case they can be written as

$$\nabla \times \mathbf{E} + \frac{\partial \mathbf{B}}{\partial t} = 0 \tag{3.1}$$

$$\nabla \times \mathbf{H} - \frac{\partial \mathbf{D}}{\partial t} = \mathbf{J}, \tag{3.2}$$

called *Faraday-Henry's* and *Maxwell-Ampere's law* respectively, together with

$$\nabla \cdot \mathbf{D} = \rho \tag{3.3}$$

$$\nabla \cdot \mathbf{B} = 0, \tag{3.4}$$

called *Gauss's* and *magnetic Gauss's law*, where $\mathbf{E}$ is the electric field intensity, $\mathbf{D}$ is the electric flux density, $\mathbf{H}$ is the magnetic field intensity, $\mathbf{B}$ is the magnetic flux density, $\mathbf{J}$ is the electric current density, and ρ is the electric charge volume density. In the international system SI the following measure units are used: [$\mathbf{E}$]=volts/meter, [$\mathbf{D}$]=coulombs/meter^2, [$\mathbf{H}$]=amperes/meter, [$\mathbf{B}$]=webers/meter^2, [$\mathbf{J}$]=amperes/meter^2 and [ρ]=coulombs/meter^3.

Maxwell's equations can also be written in integral form, as

$$\oint_\gamma \mathbf{E} \cdot d\ell = -\int_{\mathcal{S}} \frac{\partial \mathbf{B}}{\partial t} \cdot d\mathcal{S} = 0 \tag{3.5}$$

$$\oint_\gamma \mathbf{H} \cdot d\ell = \int_{\mathcal{S}} \big(\mathbf{J} + \frac{\partial \mathbf{D}}{\partial t}\big) \cdot d\mathcal{S} = 0 \tag{3.6}$$

$$\oint_{\partial\Omega} \mathbf{D} \cdot d\mathcal{S} = \int_\Omega \rho \, d\mathbf{r} \tag{3.7}$$

$$\oint_{\partial\Omega} \mathbf{B} \cdot d\mathcal{S} = 0 \tag{3.8}$$

for any open surface $\mathcal{S} \subseteq R^3$ with boundary curve $\partial\mathcal{S} = \gamma$, and for any open domain $\Omega \subseteq R^3$ having boundary surface $\partial\Omega$. Equations (3.5) and (3.6) have been obtained by integration over $\mathcal{S}$ of the curl equations (3.1) and (3.2) using Stoke's theorem, while (3.7) and (3.8) follow from the divergence equations (3.3) and (3.4) by volume integration over Ω, applying the divergence theorem. In (3.7) the contribution $Q = \int_\Omega \rho \, d\mathbf{r}$ represents the total charge stored in Ω. In the following we deal with Maxwell's equations in their differential form.

Generally, Maxwell's equations are considered together with the fundamental relation (*equation of continuity*)

$$\nabla \cdot \mathbf{J} + \frac{\partial \rho}{\partial t} = 0, \tag{3.9}$$

which specifies the conservation of charge. Only three of the five equations (3.1)-(3.4) and (3.9) are independent. Generally they are assumed to be Faraday-Henry's law, Maxwell-Ampere's law and the equation of continuity, since Gauss' s law both in the electric and in the magnetic form can be derived from them.

Maxwell's equations become a definite system of equations when *constitutive relations* describing the macroscopic properties of the materials are considered. For a simple medium they are

$$\mathbf{J} = \sigma \mathbf{E} + \mathbf{J}_s \tag{3.10}$$

$$\mathbf{D} = \epsilon \mathbf{E} \tag{3.11}$$

$$\mathbf{B} = \mu \mathbf{H}, \tag{3.12}$$

where $\mathbf{J}_s$ is the imposed source current density, σ is the electric conductivity, ϵ is the electric permittivity and μ is the magnetic permeability of the medium. The constitutive parameters σ, ϵ and μ are tensors for anisotropic media, scalars for isotropic media and they are functions of space for inhomogeneous media. Besides, for lossy media they are complex-valued.

Depending on the properties of the considered material, the permeability μ in equation (3.12) can also be function of $\mathbf{H}$. If not, i.e. $\mathbf{B}$ and $\mathbf{H}$ are linearly related, the material is called *linear*. For permanent magnets equation (3.12) assumes the modified form

$$\mathbf{B} = \mu(\mathbf{H} - \mathbf{H}_c), \tag{3.13}$$

where $\mathbf{H}_c$ is the *coercive field intensity* (i.e. the reverse magnetic field intensity that has to be applied to reduce magnetization to zero). In most cases, it is assumed that the relation between $\mathbf{B}$ and $\mathbf{H}$ is linear even for a permanent magnet. Generally, definitions $\epsilon = \epsilon_r \epsilon_0$ and $\mu = \mu_r \mu_0$ are used, with reference to the corresponding permeability $\mu_0 = 4\pi\, 10^{-7} H/m$ (henry/meter) and permittivity $\epsilon_0 = 1/(c_0^2 \mu_0) \approx 10^{-9}/(36\pi) F/m$ (farad/meter, where c_0 is the speed of light) in free space. μ_r and ϵ_r are dimensionless values associated to the material, called *relative permittivity* and *relative permeability.*

Electrostatic/magnetostatic case

When the field quantities do not vary with time, electric and magnetic properties decouple from each others and Maxwell's equations reduce to two independent systems:

$$\nabla \times \mathbf{E} = 0 \qquad (3.14)$$
$$\nabla \cdot \mathbf{D} = \rho,$$

in the electrostatic case, and

$$\nabla \times \mathbf{H} = \mathbf{J} \qquad (3.15)$$
$$\nabla \cdot \mathbf{B} = 0,$$

in the magnetostatic case. The static equation of continuity

$$\nabla \cdot \mathbf{J} = 0 \qquad (3.16)$$

is an immediate consequence of the first relation in (3.15). In the present work some magnetostatic problems derived from (3.15) will be studied.

Quasi-static case

In the time dependent case, if the time variation is sufficiently slow we can neglect the *displacement current* $\partial \mathbf{D}/\partial t$ in (3.2). This hypothesis leads to the so-called *quasi-static approximation*. Differently from the static case, nevertheless, the variation of the magnetic flux density $\mathbf{B}$ is not negligible and Faraday-Henry's equation (3.1) remains unchanged as in the general time-dependent case. Analogously to static situations, equation (3.16) holds. The quasi-static assumption is valid for problems in which frequencies are low or, more precisely, when the size of the structure is small compared with the electromagnetic wavelength associated to the highest frequency component occurring in the problem.

3.2 Boundary and interface conditions

Maxwell's equations form a system of partial differential equations with many solutions. In order to find the actual solution of the problem under consideration, we have to specify boundary conditions associated to the space domain, together with initial values in the time dependent case. In addition, interface conditions between materials have to be considered, describing the transmission of fields from one material to the other. Given two contiguous media i and j, corresponding to the disjoint domains Ω_i and Ω_j, such that $\partial\Omega_i \cap \partial\Omega_j = \Gamma_{ij} \neq \emptyset$, the transmission conditions at Γ_{ij} can be expressed as

$$\mathbf{n} \times (\mathbf{E}_i - \mathbf{E}_j) = 0 \qquad (3.17)$$
$$\mathbf{n} \times (\mathbf{H}_i - \mathbf{H}_j) = \mathbf{J}_{surf} \qquad (3.18)$$
$$\mathbf{n} \cdot (\mathbf{D}_i - \mathbf{D}_j) = \rho_{surf} \qquad (3.19)$$
$$\mathbf{n} \cdot (\mathbf{B}_i - \mathbf{B}_j) = 0, \qquad (3.20)$$

where $\mathbf{n}$ is the unit vector normal to Γ_{ij} pointing from Ω_j into Ω_i, and the quantities ρ_{surf} and $\mathbf{J}_{surf}$ are the surface charge density and the surface electric current density, respectively. The first two conditions give information about the *tangential* component of the fields $\mathbf{E}$ and $\mathbf{H}$: the former is continuous, the latter is discontinuous if surface currents exist. The last two conditions describe the *normal* component of $\mathbf{D}$ and $\mathbf{B}$, respectively discontinuous if surface charges exist, and continuous.

Of these four conditions only two are independent, for instance (3.17) and (3.18). The condition (3.17) for the tangential component of $\mathbf{E}$ is equivalent to the condition (3.20) for the normal component of $\mathbf{B}$, while the condition (3.18) for the tangential component of $\mathbf{H}$ corresponds to (3.19) for the normal component of $\mathbf{D}$. In the quasi-static approximation, where $\nabla \cdot \mathbf{J} = 0$, also the condition

$$\mathbf{n} \cdot (\mathbf{J}_i - \mathbf{J}_j) = 0 \tag{3.21}$$

has to be considered, describing the continuity of the normal component of the current density at the interface Γ_{ij}. Some special cases can be considered.

Interface between two lossless media

In this case no surface currents and no free surface charges exist at the interface, and conditions become homogeneous:

$$\mathbf{n} \times (\mathbf{E}_i - \mathbf{E}_j) = 0 \tag{3.22}$$
$$\mathbf{n} \times (\mathbf{H}_i - \mathbf{H}_j) = 0 \tag{3.23}$$
$$\mathbf{n} \cdot (\mathbf{D}_i - \mathbf{D}_j) = 0 \tag{3.24}$$
$$\mathbf{n} \cdot (\mathbf{B}_i - \mathbf{B}_j) = 0, \tag{3.25}$$

describing continuity at Γ_{ij} for all the components E_t, H_t, D_n and B_n.

Interface between a dielectric and a perfect conductor

The above conditions can be reduced to a special case when one of the two media approximates a perfect conductor, i.e. has conductivity $\sigma \to \infty$. Since in the time-varying case a perfect conductor cannot sustain any field in its *interior*, equations (3.17)-(3.20) become

$$\mathbf{n} \times \mathbf{E} = 0 \tag{3.26}$$
$$\mathbf{n} \times \mathbf{H} = \mathbf{J}_{surf} \tag{3.27}$$
$$\mathbf{n} \cdot \mathbf{D} = \rho_{surf} \tag{3.28}$$
$$\mathbf{n} \cdot \mathbf{B} = 0, \tag{3.29}$$

where $\mathbf{E}$, $\mathbf{H}$, $\mathbf{D}$ and $\mathbf{B}$ are the fields exterior to the conductor and $\mathbf{n}$ is the normal unit vector pointing away from the conductor.

Boundary conditions

Given a bounded material domain Ω, conditions at the boundary $\Gamma = \partial\Omega$ have to be modelled considering that what is mathematically a "boundary" is nothing but an interface with an *external* medium whose electromagnetic status is already known. This means that fields or their normal or tangential components are given data on the several parts of Γ. Boundary data have, of course, to be assigned in a consistent way so that they are compatible with each other. A choice, coherently with (3.17)-(3.20), is to assume the following quantities as known:

$$\mathbf{n} \times \mathbf{E} \quad \text{or} \quad \mathbf{n} \cdot \mathbf{B} \quad \text{on } \Gamma_1 \tag{3.30}$$

$$\mathbf{n} \times \mathbf{H} \quad \text{or} \quad \mathbf{n} \cdot \mathbf{D} \quad \text{on } \Gamma_2, \tag{3.31}$$

where $\Gamma_1 \subseteq \Gamma$ and $\Gamma_2 \subseteq \Gamma$ are such that $\Gamma_1 \cup \Gamma_2 = \Gamma$, e. g. by giving equation (3.26) or (3.29) on Γ_1, and (3.27) or (3.28) on Γ_2. In case of unbounded domains, a formal approach would be to consider limit conditions at infinite distances, nevertheless any modelling for computational purposes (e.g. finite element methods) requires necessarily an approximation of the infinite geometry with a finite one, by introduction of fictitious boundaries at "sufficiently" big distances.

3.3 Scalar and vector potentials

Until now, electromagnetic equations have been considered in the form of first order differential equations involving the vectors **E**, **H**, **D** and **B**. When an electromagnetic problem is described by these vector fields, it is said that a *field formulation* is used. In field formulations, the constitutive relations (3.10)-(3.13) allow to express equations in terms of only two field quantities, e.g. **E** and **B**, or **E** and **H**.

A different approach can be to convert a first order differential problem involving two field quantities into a second order problem involving only one field quantity. This is made possible by introducing proper scalar or vector potentials. In such a case, it is said that a *potential formulation* is used. Several formulations can be given, in which potentials can be defined separately or combined together in different regions of the domain, according to the nature of the problem and the topological properties of such regions. Some potential formulations are mentioned in the following.

Scalar electric potential and vector magnetic potential

Owing to the magnetic Gauss's law, the vector field **B** is solenoidal (zero divergence) in the whole simply connected space. It is then possible to express it in terms of a *vector magnetic potential*, i.e. a differentiable vector function **A** such that

$$\mathbf{B} = \nabla \times \mathbf{A}. \tag{3.32}$$

Then, from Faraday's law and definition (3.32), it follows that

$$\nabla \times \big(\mathbf{E} + \frac{\partial \mathbf{A}}{\partial t}\big) = 0, \tag{3.33}$$

again considered in the whole space. Since irrotational fields on simply connected domains are conservative, we can introduce a *scalar electric potential* V, defined as

$$-\nabla V = \mathbf{E} + \frac{\partial \mathbf{A}}{\partial t}, \tag{3.34}$$

which is the generalization of the classical relation $\mathbf{E} = -\nabla V$ used in the static case. Electrostatic problems can then be studied by solving V in the *electric Poisson's equation*

$$\nabla \cdot (\epsilon \nabla V) = -\rho, \tag{3.35}$$

derived from Gauss's law when applying the static definition of V.

In general, neither $\mathbf{A}$ nor V are uniquely defined. It is known from Helmhotz's theorem that the definition of one vector requires the specification of both its curl and its divergence, therefore a further condition on the divergence of $\mathbf{A}$ has to be imposed (*gauging*). This gauge condition is chosen so that proper terms vanish in the formulation of Maxwell's equations by the vector potential $\mathbf{A}$. For static problems, the simplest condition is the so-called *Coulomb gauge*

$$\nabla \cdot \mathbf{A} = 0, \tag{3.36}$$

which makes $\mathbf{A}$ and V well-defined up to an additive constant. Rewriting the static Maxwell-Ampere's equation by definition (3.32), and using gauge (3.36), we get the *vector Poisson's equation*

$$\nabla^2 \mathbf{A} = -\mu \mathbf{J} \tag{3.37}$$

for magnetostatic problems. For time dependent problems, a more convenient choice is the so-called *Lorentz gauge* expressed by

$$\nabla \cdot \mathbf{A} = -\mu\epsilon \frac{\partial V}{\partial t}, \tag{3.38}$$

which reduces to the Coulomb gauge for the static case. See [16] or [44] for details about gauging and the corresponding expressions of the time dependent Maxwell's equations in terms of potentials $\mathbf{A}$ and V. A formulation by the vector $\mathbf{A}$ is appropriate for 2D problems, because $\mathbf{A}$ is orthogonal to the domain, e.g. $\mathbf{A} = A_z\,\mathbf{i}$ for problems defined on the xy-plane.

Vector electric potential and scalar magnetic potential

As alternative to the **A**-V formulation, in the quasi-static case it is possible to introduce other scalar and vector potentials. Since the current density **J** is solenoidal in space, there exists in fact a vector **T**, called *vector electric potential*, such that

$$\mathbf{J} = \nabla \times \mathbf{T}. \tag{3.39}$$

Therefore, substituting (3.39) in Maxwell-Ampere's law, we have

$$\nabla \times (\mathbf{H} - \mathbf{T}) = 0, \tag{3.40}$$

so that a *scalar magnetic potential* χ can be introduced with definition

$$\mathbf{H} = \mathbf{T} - \nabla\chi. \tag{3.41}$$

Field equations can then be expressed in terms of **T** by considering Faraday-Henry's law and the magnetic Gauss's law, the constitutive relations **J**-**E** and **B**-**H**, and definitions (3.39) and (3.41). As a result, we get

$$\nabla \times (\frac{1}{\sigma}\nabla \times \mathbf{T}) + \mu\frac{\partial}{\partial t}(\mathbf{T} - \nabla\chi) = \nabla \times \big(\frac{1}{\sigma}\mathbf{J}_s\big) \tag{3.42}$$

and

$$\nabla \cdot (\mathbf{T} - \nabla\chi) = 0. \tag{3.43}$$

Note that **T** and χ are not unique and, analogously to **A**, a gauge condition has to be specified. Possible gauges for **T** are the Coulomb gauge, requiring zero divergence for **T**, or the Lorentz gauge

$$\nabla \cdot \mathbf{T} = \sigma\mu\frac{\partial\chi}{\partial t}, \tag{3.44}$$

or the condition

$$\mathbf{T} \cdot \mathbf{u} = 0, \tag{3.45}$$

where **u** is an arbitrary vector field that does not have closed field lines [45].

In both the **A**-V and **T**-χ formulations, boundary and interface conditions (3.30)-(3.31) and (3.17)-(3.20) have to be expressed in terms of the scalar and vector potentials [44].

Further formulations of Maxwell's equations could be introduced in terms of potential quantities and mixed approaches could be considered in different parts of the domain. In the next section, we present an alternative formulation based on the notion of two different scalar magnetic potentials, as it has been used in the present work to describe some 3D magnetostatic models.

3.4 Scalar potentials for magnetostatic problems

In three-dimensional static problems, $\mathbf{A}$ and $\mathbf{T}$ present a full vector form that is not very efficient in most cases. Similarly to the electrostatic case where a V-formulation is generally used for 3D models, in magnetostatic problems it is convenient to introduce two suitable scalar magnetic potentials φ and ϕ, which are defined separately in two different regions of the domain, depending whether regions contain currents or not.

From Helmhotz's theorem the magnetic field intensity $\mathbf{H}$ can be always partitioned as

$$\mathbf{H} = \mathbf{H}_s + \mathbf{H}_m, \tag{3.46}$$

where $\mathbf{H}_s$ is solenoidal and represents the magnetic field intensity due to prescribed source currents, while $\mathbf{H}_m$ is irrotational and describes the magnetic field intensity due to induced magnetization in materials. It is possible then to define a scalar potential φ, called *reduced magnetic potential*, such that

$$\mathbf{H} = -\nabla\varphi + \mathbf{H}_s, \tag{3.47}$$

in which the source field $\mathbf{H}_s$ can be computed using the *Biot-Savart law*. Given a source current density $\mathbf{J}_s$ defined on a conductor domain Ω_s, called *source region*, such law tells that the resulting field $\mathbf{H}_s = \mathbf{H}_s(\mathbf{r})$ is given by

$$\mathbf{H}_s = \frac{1}{4\pi}\int_{\Omega_s} \mathbf{J}_s \times \nabla\Big(\frac{1}{\mid \mathbf{r}-\mathbf{r}' \mid}\Big)\ d\mathbf{r}' \tag{3.48}$$

or, equivalently,

$$\mathbf{H}_s(\mathbf{r}) = \frac{1}{4\pi}\int_{\Omega_s} \mathbf{J}_s \times \frac{\mathbf{r}-\mathbf{r}'}{\mid \mathbf{r}-\mathbf{r}' \mid^3}\quad d\mathbf{r}', \tag{3.49}$$

where $\mathbf{r}$ is an arbitrary point in space (called *field point*) and $\mathbf{r}'$ is any point in Ω_s (called *source point*). An overview of various techniques for the computation of the Biot-Savart law is presented in [44]. For simple current-carrying geometries like bars and coils with polygonal cross section, etc., analytical expressions have been derived by L.U. Urankar [46, 47, 48]. Some of these numerical or semi-analytical techniques have been implemented on test cases studied in Chapter 7. See details in [27].

Under these premises, considering the magnetic Gauss's law and the constitutive relations (3.12) and (3.13), the following *magnetic Poisson's equation* follows

$$\nabla\cdot(\mu\nabla\varphi) = -\nabla\cdot\mu\mathbf{H}_c + \nabla\cdot\mu\mathbf{H}_s, \tag{3.50}$$

in which also permanent magnets with coercive field $\mathbf{H}_c$ have been modelled.

For static and quasi-static problems, it is possible to introduce another scalar potential on simply connected domains where no source regions Ω_s are present. Since $\nabla \times \mathbf{H} = 0$ on such domains, a scalar potential ϕ can be introduced such that

$$\mathbf{H} = -\nabla\phi, \tag{3.51}$$

called *total magnetic potential.* On regions with no source currents, we get then the equation

$$\nabla \cdot (\mu \nabla \phi) = -\nabla \cdot \mu \mathbf{H}_c, \tag{3.52}$$

which reduces to Laplace's equation when there are no permanent magnets.

Given a domain Ω with source regions $\Omega_s \subseteq \Omega$, instead of considering only the potential φ, an alternative approach could be to use both ϕ and φ. If the topology of the domain makes it possible, the idea is to partition Ω in two parts: a subdomain Ω_{red} such that $\Omega_s \subseteq \Omega_{red}$, where the reduced potential φ and then (3.50) will be used, and a simply connected subdomain Ω_{tot}, where the total potential ϕ and (3.52) will be used. In this section, for brevity, Ω_{tot} is called the *total domain* and Ω_{red} the *reduced domain.* The advantage of such *double potential formulation*, differently from a complete formulation in φ, lies in the reduction of some cancellation errors that would occur in the reduced domain when computing the total field $\mathbf{H}$ by (3.47), especially for large permeabilities μ.

Boundary and interface conditions have then to be expressed in terms of the two potentials ϕ and φ. By convection, we first assume that possible permanent magnet regions are contained in the total domain. Let $\Gamma_I = \partial\Omega_{red} \cap \partial\Omega_{tot}$ be the interface between the reduced and the total domain. From (3.20), using the definitions of ϕ and φ and the constitutive relations between $\mathbf{B}$ and $\mathbf{H}$, we get the first total/reduced interface condition

$$(\mu_{red}\nabla\varphi - \mu_{tot}\nabla\phi) \cdot \mathbf{n} = (\mu_{red}\mathbf{H}_s + \mu_{tot}\mathbf{H}_c) \cdot \mathbf{n} \qquad \text{on } \Gamma_I, \tag{3.53}$$

where $\mathbf{n}$ is the normal unit vector at Γ_I, whose direction can be arbitrarily chosen. To obtain the second interface condition, we rewrite (3.18) in terms of ϕ and φ and have

$$[\nabla(\varphi - \phi) - \mathbf{H}_s] \times \mathbf{n} = 0, \tag{3.54}$$

hence

$$\nabla(\varphi - \phi) \cdot \mathbf{t} = \mathbf{H}_s \cdot \mathbf{t} \qquad \text{on } \Gamma_I, \tag{3.55}$$

where $\mathbf{t}$ is the unit tangent vector at Γ_I. We first assume that Γ_I is connected. Then, fixed arbitrarily a point $\mathbf{r}_0 \in \Gamma_I$, we integrate over any piecewise regular path $\gamma[\mathbf{r}_0, \mathbf{r}] \subseteq \Gamma_I$ for any point $\mathbf{r} \in \Gamma_I$, and get the second total/reduced interface condition

$$\phi(\mathbf{r}) = \varphi(\mathbf{r}) - \int_{\mathbf{r}_0}^{\mathbf{r}} \mathbf{H}_s \cdot d\mathbf{r} \qquad \text{on } \Gamma_I, \tag{3.56}$$

where it is assumed $\phi(\mathbf{r}_0) = \varphi(\mathbf{r}_0)$. Condition (3.56) describes a jump of discontinuity between total and reduced potential values at the interface, due to the source field. If Γ_I is disconnected, a condition like (3.56) has to be repeated on each single connected component.

When permanent magnets are considered in the total domain, interface conditions between permanent and soft materials have also to be included. If $\Omega_1 \subseteq \Omega_{tot}$ is a soft material with permeability μ_1 adjacent to a permanent magnet $\Omega_2 \subseteq \Omega_{tot}$ with permeability μ_2, the interface conditions become

$$(\mu_1 - \mu_2)\nabla\phi \cdot \mathbf{n} = \mu_2 \mathbf{H}_c \cdot \mathbf{n} \tag{3.57}$$

$$\phi_{(1)} = \phi_{(2)}, \qquad \text{on } \Gamma_{12}, \tag{3.58}$$

with $\Gamma_{12} = \partial\Omega_1 \cap \partial\Omega_2$, where $\phi_{(1)}$ and $\phi_{(2)}$ denote the values (or limit values) of ϕ on Γ_{12} from the sides of Ω_1 and Ω_2 respectively. In the simpler case in which both Ω_1 and Ω_2 are soft materials, relations similar to (3.57) and (3.58) hold, now with $\mathbf{H}_c = 0$, so that also the first condition becomes homogeneous. Possible interface conditions between two soft materials in the reduced domain are expressed in analogous way, by changing ϕ with φ.

In a similar way, boundary conditions are obtained. We call Γ_N and Γ_D the parts of $\Gamma = \partial\Omega$ on which, respectively, the normal and tangential components of the magnetic field are assigned (one of the two can be empty) and suppose that the reduced domain $\overline{\Omega}_{red}$ intersects the boundary. Then, we get the non-homogeneous Neumann condition

$$\nabla\varphi \cdot \mathbf{n} = \mathbf{H}_s \cdot \mathbf{n} \qquad \text{on } \Gamma_{N,red}, \tag{3.59}$$

where $\Gamma_{N,red} = \partial\Omega_{red} \cap \Gamma_N$, when it is non-empty. Besides, if $\Gamma_{D,red} = \Omega_{red} \cap \Gamma_D$ is non-empty and connected, we get the non-homogeneous Dirichlet condition

$$\varphi(\mathbf{r}) = \int_{\mathbf{r}_A}^{\mathbf{r}} \mathbf{H}_s \cdot d\mathbf{r}, \quad \varphi(\mathbf{r}_A) = 0 \quad \text{on } \Gamma_{D,red} \tag{3.60}$$

where $\mathbf{r}_A \in \Gamma_{D,red}$ is a point fixed arbitrarily. If $\Gamma_{D,red}$ is disconnected, a condition like (3.60) has to be given on each single connected component. Similarly, we consider now the total domain $\overline{\Omega}_{tot}$ when it intersects the boundary. The Neumann condition takes the form

$$\mu_{tot}\nabla\phi \cdot \mathbf{n} = -\mu_{tot}\mathbf{H}_c \cdot \mathbf{n} \qquad \text{on } \Gamma_{N,tot}, \tag{3.61}$$

with $\Gamma_{N,tot} = \partial\Omega_{tot} \cap \Gamma_N$, when it is non-empty. If $\Gamma_{D,tot} = \Omega_{tot} \cap \Gamma_D$ is non-empty and connected, we get a non-homogeneous constant Dirichlet condition. In particular, when

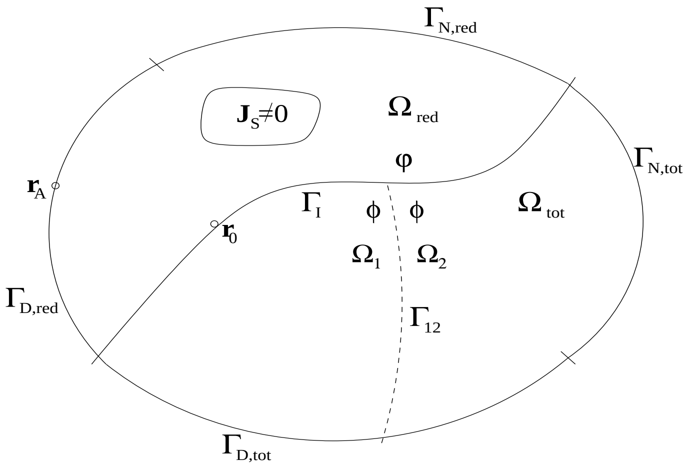

Figure 1: A two-dimensional domain with total and reduced regions

$\Gamma_{D,tot} \cup \Gamma_I \cup \Gamma_{D,red}$ is connected and condition (3.60) is imposed on $\Gamma_{D,red}$, for consistency we have to fix the condition

$$\phi(\mathbf{r}) = \int_{\mathbf{r}_A}^{\mathbf{r}_0} \mathbf{H}_s \cdot d\mathbf{r} \quad \text{on } \Gamma_{D,tot}. \tag{3.62}$$

In the other cases, one may specify

$$\phi(\mathbf{r}) = \phi(\mathbf{r}_B) \quad \text{on } \Gamma_{D,tot}, \tag{3.63}$$

where $\mathbf{r}_B$ is a point fixed arbitrarily in $\Gamma_{D,tot}$, assuming for instance $\phi(\mathbf{r}_B) = 0$. See in Figure 1 a possible 2D schematic representation of the domain, in the simpler case in which both Γ_N and Γ_D are connected.

Section 4.4 presents the complete analytical form of a 3D boundary value problem obtained from the above double potential formulation, to describe magnetostatic models composed of soft magnetic materials with imposed currents. For a more detailed overview of electromagnetic fields and potentials, see [16, 28] and [44, 45].

4 The model: definition and finite element analysis

4.1 The abstract model

Let us first introduce in its abstract framework the class of boundary value problems studied in the present paper.

Let $\Omega_1 \subseteq R^3$ and $\Omega_2 \subseteq R^3$ be two *open*, disjoint, bounded and connected domains, Lebesgue measurable with Lipschitz continuous boundaries $\partial\Omega_1$ and $\partial\Omega_2$. We assume they are *adjacent*, i.e. the set $\Gamma_I = \partial\Omega_1 \cap \partial\Omega_2$ is a non-empty surface (called *interface*). Let us denote by $\Omega = \overline{\Omega_1 \dot{\cup} \Omega_2}$ the open global domain. We here consider the following class of second order boundary-interface value problems:

$$\begin{cases} -\nabla \cdot (\alpha \nabla u) = f & \text{in } \Omega \\ u_1 = u_2 + d & \text{on } \Gamma_I \\ \alpha_1 \nabla u_1 \cdot \mathbf{n}_1 + \alpha_2 \nabla u_2 \cdot \mathbf{n}_2 = p & \text{on } \Gamma_I \\ u = u_D & \text{on } \Gamma_D \\ \alpha \nabla u \cdot \mathbf{n} = q & \text{on } \Gamma_N, \end{cases} \tag{4.1}$$

where $\Gamma_D \subseteq \Gamma$ and $\Gamma_I \subseteq \Gamma$ are parts of the boundary $\Gamma = \partial\Omega$, such that $\Gamma_D \cup \Gamma_N = \Gamma$.

Problem (4.1) is a generalized Poisson model with mixed non-homogeneous Dirichlet-Neumann boundary and interface conditions in the unknown $u = u(x, y, z)$. $\mathbf{n}_i$ and $\mathbf{n}$ denote the normal unit vectors at Γ_I and Γ pointing towards the exterior of the domains Ω_i, $i = 1, 2$, and Ω respectively, while u_i and α_i denote the values (or limit values) on Γ_I of the functions u and α from the sides of each Ω_i, $i = 1, 2$. The (real-valued) functions $\alpha = \alpha(x, y, z)$ and $f = f(x, y, z)$ defined on Ω, $d = d(x, y, z)$ and $p = p(x, y, z)$ on Γ_I, $q = q(x, y, z)$ on Γ_N and $u = u_D(x, y, z)$ on Γ_D are given data satisfying certain regularity properties. For the following, we assume that the diffusion coefficient $\alpha = \alpha(x, y, z)$ is a positive bounded function on Ω, Lipschitz continuous over each Ω_i, so that the linear Poisson operator $\mathcal{L}u = -\nabla \cdot (\alpha \nabla u)$ in (4.1) is uniformly elliptic on Ω. Further, we assume that (4.1) has a unique solution.

Our intention, in this Chapter, is to derive a variational formulation of problem (4.1) for a finite element analysis, to be applied to some 3D magnetostatic models that can be viewed as particular cases of (4.1).

4.2 Variational formulation

Under *weak* conditions of regularity for f, d, p, q and u_D, we derive a variational formulation of model (4.1). Let us assume $f \in L_2(\Omega)$, $p \in L_2(\Gamma_I)$, $q \in L_2(\Gamma_N)$, $d \in H^{1/2}(\Gamma_I)$ and $u_D \in H^{1/2}(\Gamma_D)$. We obtain then the weak form of (4.1) by a formal procedure similar to the one applied to the classical Poisson model with no interfaces [37], considering both domains Ω_1 and Ω_2. Thus, we multiply the differential equation in (4.1) by an arbitrary $v \in H_{0,\Gamma_D}(\Omega)$ and integrate over each Ω_i, $i = 1, 2$. Then, we apply Green's theorem to the two integral equalities and split the corresponding surface integrals over $\partial\Omega_i$ in the several parts of Γ_D, Γ_N and Γ_I defined by the relation

$$\partial\Omega_i = (\partial\Omega_i \cap \Gamma_D) \cup (\partial\Omega_i \cap \Gamma_N) \cup (\partial\Omega_i \cap \Gamma_I), \quad i = 1, 2. \tag{4.2}$$

Finally, using Neumann conditions both at the interface and the boundary and summing up the two equalities, we get the following weak form for problem (4.1):

(variational formulation) *Find* $u = u(x, y, z) \in L_2(\Omega)$, *where* $u\,|_{\Omega_i} = u_i \in H^1(\Omega_i)$ *for* $i = 1, 2$, *such that*

$$\int_\Omega \alpha \nabla u \cdot \nabla v d\mathbf{x} = \int_\Omega f v \; d\mathbf{x} + \int_{\Gamma_N} qv \; d\mathcal{S} + \int_{\Gamma_I} pv \; d\mathcal{S}, \qquad \forall v \in H^1_{0,\Gamma_D}(\Omega), \tag{4.3}$$

and such that $u = u_D$ *on* Γ_D *and* $u_1 = u_2 + d$ *on* Γ_I *(in the sense of trace).*

In this model with interfaces, the solution $u = u(x, y, z)$ belongs to $L_2(\Omega)$ but not to $H^1(\Omega)$, because of the presence of a non-zero jump function d on Γ_I in the first interface condition of (4.1). Thus, as a natural setting for our weak solution it makes sense to introduce the following *piecewise* Sobolev space

$$H^1(\Omega_1, \Omega_2) = \{w \in L_2(\Omega) : w\,|_{\Omega_i} \in H^1(\Omega_i), i = 1, 2\}. \tag{4.4}$$

Denoting by $w_i = w\,|_{\Omega_i}$, for $i = 1, 2$, the component functions of any $w \in H^1(\Omega_1, \Omega_2)$, the definition

$$\| w \|_{H^1(\Omega_1,\Omega_2)} = \| w_1 \|_{H^1(\Omega_1)} + \| w_2 \|_{H^1(\Omega_2)} \tag{4.5}$$

can be then chosen as a natural norm. Coherently, we introduce the subspace $H^1_{0,\Gamma_D}(\Omega_1, \Omega_2)$ of functions $w \in H^1(\Omega_1, \Omega_2)$ whose trace γw on Γ_D vanishes. Similarly to spaces $H^1_0(\Omega)$ and $H^1_{0,\Gamma_D}(\Omega)$, for each $w \in H^1_{0,\Gamma_D}(\Omega_1, \Omega_2)$ it is easy to prove that the definition

$$\| w \|_{H^1_{0,\Gamma_D}(\Omega_1,\Omega_2)} = \| w_1 \|_{H^1_{0,\Gamma_D}(\Omega_1)} + \| w_2 \|_{H^1_{0,\Gamma_D}(\Omega_2)} \tag{4.6}$$

is another norm for $H^1_{0,\Gamma_D}(\Omega_1, \Omega_2)$ together with the induced norm from (4.5), with w_i as component functions of w on Ω_i, $i = 1, 2$.

In (4.3), differently from the solution $u \in H^1(\Omega_1, \Omega_2)$, the test functions v belong to $H^1_{0,\Gamma_D}(\Omega) \subseteq H^1(\Omega)$, so that their trace γv is well-defined in Γ_I and Γ. Similarly to models without any interface conditions, it can be shown immediately that (4.3) is equivalent to the weak formulation of a model with Dirichlet boundary conditions that are *homogeneous* on Γ_D and such that *no jumps exist at the interface* Γ_I. Regarding this, let us consider the substitution

$$u = \tilde{u} + \tilde{u}_D, \tag{4.7}$$

where $\tilde{u}_D$ is an extension of u_D on Ω such that $\tilde{u}_D \in H^1(\Omega_1, \Omega_2)$ and the component functions $\tilde{u}_{D,1}$ on Ω_1 and $\tilde{u}_{D,2}$ on Ω_2 satisfy the condition $\tilde{u}_{D,1} = \tilde{u}_{D,2} + d$ on Γ_I. Then, it results $\tilde{u} \in H^1_{0,\Gamma_D}(\Omega)$. Now we introduce the bilinear form

$$a(w,v) = \int_\Omega \alpha \nabla w \cdot \nabla v \, d\mathbf{x} \qquad \forall w, v \in H^1_{0,\Gamma_D}(\Omega), \tag{4.8}$$

and, for a fixed function ϱ Lebesgue measurable on a surface $\mathcal{S} \subseteq \partial\Omega$, the following notation of linear functional

$$< \varrho, v >_{\mathcal{S}} = \int_{\mathcal{S}} \varrho v \; d\mathcal{S} \qquad \forall v \in H^1_{0,\Gamma_D}(\Omega). \tag{4.9}$$

Then, denoting by $(\cdot,\cdot)_\Omega$ the usual L_2-scalar product on Ω, from (4.3) we get the following

(equivalent variational formulation) *Find* $\tilde{u} \in H^1_{0,\Gamma_D}(\Omega)$ *such that*

$$a(\tilde{u}, v) = b(v) \qquad \forall v \in H^1_{0,\Gamma_D}(\Omega), \tag{4.10}$$

where a *is given by* (4.8) *and*

$$b(v) = (f, v)_\Omega - (\alpha \nabla \tilde{u}_D, \nabla v)_\Omega + < q, v >_{\Gamma_N} + < p, v >_{\Gamma_I}, \tag{4.11}$$

with $< q, \cdot >_{\Gamma_N}$ *and* $< p, \cdot >_{\Gamma_I}$ *given by* (4.9).

The advantage of this equivalent formulation is that now the sought weak solution vanishes on Γ_D like the test functions v, and its component functions $\tilde{u}_i$ satisfy the condition $\tilde{u}_1 = \tilde{u}_2$ on Γ_I. The non-zero value at the Dirichlet boundary and the discontinuity at the interface have been transferred to a known function $\tilde{u}_D$.

Good properties hold for a and b. First, a is symmetric and continuous, i.e.

$$| a(w,v) | \leq C_1 \parallel w \parallel_{H^1_{0,\Gamma_D}(\Omega)} \parallel v \parallel_{H^1_{0,\Gamma_D}(\Omega)} \quad \forall w, v \in H^1_{0,\Gamma_D}(\Omega), \tag{4.12}$$

as it follows from the Cauchy-Schwartz inequality, by taking $C_1 = \parallel \alpha \parallel_{L_\infty}$ (here, equal to $\max_\Omega \alpha$). Then, due to the uniform ellipticity, we have

$$a(v,v) \geq C_2 \parallel v \parallel^2_{H^1_{0,\Gamma_D}(\Omega)} \quad \forall v \in H^1_{0,\Gamma_D}(\Omega) \tag{4.13}$$

with $C_2 = \min_\Omega \alpha$ (in such a case, it is said that a is *coercive* on $H^1_{0,\Gamma_D}(\Omega)$). Besides, the linear operator b is continuous, i.e.

$$| b(v) | \leq C_3 \parallel v \parallel_{H^1_{0,\Gamma_D}(\Omega)} \quad \forall v \in H^1_{0,\Gamma_D}(\Omega), \tag{4.14}$$

as it follows from the boundedness property of the functionals $(f,v)_\Omega$, $(\alpha\nabla\tilde{u}_D, \nabla v)_\Omega$, $<q,v>_{\Gamma_N}$ and $<p,v>_{\Gamma_I}$, using Cauchy-Schwartz and Poincaré's inequalities, with $C_3 > 0$ depending on α, f, p, q, $\tilde{u}_D$, Ω_1 and Ω_2. Thus, from the Lax-Milgram theorem [22, 37], there exists a unique weak solution for the variational problem (4.10), as well as (4.3).

To conclude, property (4.13) guarantees that $a(v,v) \geq 0$, for each $v \in H^1_{0,\Gamma_D}(\Omega)$ (the property holds also in a larger space, like $H^1(\Omega)$). We can therefore introduce the equivalent norm

$$\parallel v \parallel_{\mathcal{E},\Omega} = \sqrt{a(v,v)} = \Big(\int_\Omega \alpha \nabla v \cdot \nabla v \, d\mathbf{x} \Big)^{1/2}, \tag{4.15}$$

which will be used many times in the following, called *energy norm*.

4.3 Finite element discretization

For a finite element discretization of the variational equation (4.3), let $T_h = \{\tau\}$ be a *conformal* 3D triangulation of Ω, i.e. a partition of Ω in open triangular subdomains τ pairwise disjoint or having either a vertex, an edge or a face in common, such that $\overline{\Omega} = \bigcup \overline{\tau}$. Let us suppose that T_h is also *constrained* at the interface Γ_I, i.e. each element is disjoint from Γ_I or has a vertex, an edge or a face lying on it. The index h, called *mesh size*, measures the pointwise size of the elements in the triangulation, and has to satisfy some regularity properties. Typically, h is defined as the piecewise constant positive function such that $h\,|_\tau = \operatorname{diam}(\tau)$ for any element τ, i.e. it equals the longest edge of τ. Weaker assumptions for h can however be suggested. For instance, defining $h_\tau = \operatorname{diam}(\tau)$ for each $\tau \in T_h$, C. Johnson and K. Eriksson require in [21] that:

1) $h \in C^1(\overline{\Omega})$, it is positive and there exists $\nu > 0$ such that

$$| \nabla h(\mathbf{x}) | \leq \nu, \quad \forall x \in \overline{\Omega}; \tag{4.16}$$

2) there exists a constant $c_1 > 0$ such that

$$c_1 h_\tau^3 \leq \int_\tau d\mathbf{x}, \quad \forall \tau \in T_h; \tag{4.17}$$

3) there exists a constant $c_2 > 0$ such that

$$c_2 h_\tau \leq h(\mathbf{x}) \leq h_\tau, \quad \forall x \in \tau, \ \forall \tau \in T_h. \tag{4.18}$$

By means of these conditions it is required to have a sufficiently "good" mesh, that is: 1) sufficiently uniform with a not too large variation in size among the elements, 2) with not too sharp angles in the elements, and 3) whose element shapes are not too far from the equilateral one. In [11] and [15] it is explained how the quality of the element shapes in the triangulation can affect the convergence of finite element solutions.

We can now turn to the discretization of (4.10), by using a *continuous Galerkin* finite element method. Let $V_h^r \subseteq H^1_{0,\Gamma_D}(\Omega)$ be the finite-dimensional space of continuous functions piecewise defined on Ω, vanishing on Γ_D, that are continuous polynomials of order r over each element in T_h. Then, by definition, the Galerkin finite element solution satisfies the variational form (4.10) for test functions considered in this finite-dimensional space, i.e. the following problem:

(discrete variational formulation) *Find $\tilde{u}_h \in V_h^r$ such that*

$$a(\tilde{u}_h, v_h) = b(v_h) \qquad \forall v_h \in V_h^r, \tag{4.19}$$

where a and b are defined by (4.8) *and* (4.11).

The discrete model $A\mathbf{u} = \mathbf{b}$ is then derived in a similar manner to models without interface. It is sufficient to impose the discrete condition (4.19) on test functions v_h belonging to the same finite-dimensional basis in V_h^r used for the finite representation of the discrete solution. The basis functions are chosen so that a local compact support property holds (e.g. in the piecewise linear case, the well-known *hat-functions* can be used). Together with the interior sources and the boundary conditions, in our case a contribution from the interface conditions has to be included in the right hand side $\mathbf{b}$. If a piecewise linear Galerkin method is applied, for instance, the number of degrees of freedom for the linear system is the number n of the interior and Neumann boundary nodes defined by the triangulation T_h, with interface nodes included (called *free nodes*). In the definition of the discrete model, the interface condition $u_1 = u_2 + d$ is inserted into the structure of the linear system, in order to compute directly the finite element approximation u_h of the solution u, instead of $\tilde{u}_h$. In the unknown vector $\mathbf{u} = (\widehat{u}_1, \widehat{u}_2, \cdots, \widehat{u}_n)^T$, the generic component $\widehat{u}_i = u_h(x_i, y_i, z_i)$ represents the value of the finite element solution u_h at the i-th free node of T_h. The components of $\mathbf{u}$ on nodes belonging to Γ_I are associated either to the function u_1 or to u_2, by arbitrary convention, as the value of the other one is derived immediately from the knowledge of the jump d.

Owing to the uniform ellipticity of the form $a(u, v)$, the stiffness matrix is non-singular, symmetric, positive definite and, due to the local support property, sparse. Therefore, the linear system is generally solved by iterative methods, e.g. Krylov subspace methods. Suitable preconditioners $\mathbf{B}$ can be applied in order to reduce from $\kappa(\mathbf{A})$ to $\kappa(\mathbf{BA})$ the

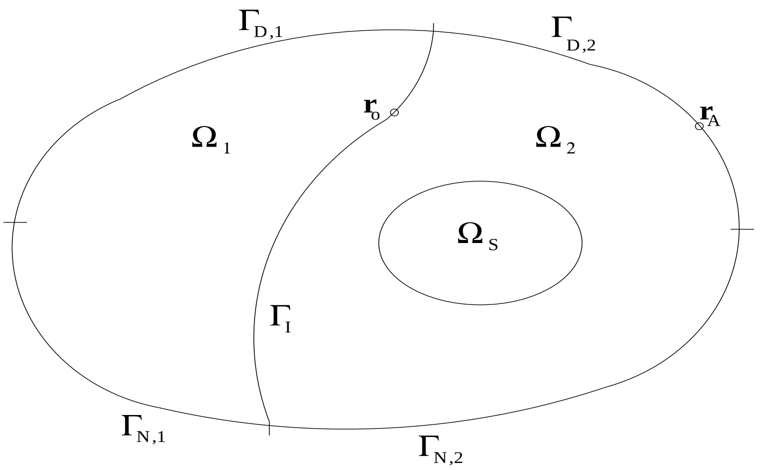

Figure 2: A two-dimensional projection of the model domain

condition number of the stiffness matrix, which would otherwise grow as the mesh size becomes finer. In [13] X. Cai and K. Samuelsson suggest some methods, like additive Schwartz methods and multigrid techniques, that can be used as possible preconditioners for the stiffness matrix. Aspects about the implementation of the discrete model (4.19), in our specific applications for magnetostatic problems, will be described in Chapter 6.

4.4 A magnetostatic problem

The electromagnetic model studied in the present work is a particular case of the general boundary value problem (4.1) for special values of the data functions f, d, p, q and u_D related to magnetic properties.

In the following, when omitted, it is always intended that all material regions, all boundaries and interfaces satisfy the"good" properties of regularity specified in Section 4.1. The intention is now to investigate the behaviour of magnetic fields in static conditions in a region of space containing prescribed currents. Let $\Omega \subseteq R^3$ be the region of interest with boundary Γ, composed of materials that are soft media, all linear, homogeneous and isotropic, so that the magnetic permeability μ is a piecewise constant positive function, i.e. constant on each material. Let us suppose that there exists a conductor domain $\Omega_s \subseteq \Omega$ where a current flows with density $\mathbf{J}_s$. Let us partition the domain in two material regions Ω_1 and Ω_2 such that Ω_2 contains Ω_s and Ω_1 is simply connected, and denote by $\Gamma_I = \partial\Omega_1 \cap \partial\Omega_2$ the interface between them. Each of the domains Ω_i can be composed of several materials.

According to the double potential formulation presented in Section 3.4, we can now write Maxwell's equations in terms of a total magnetic potential ϕ on Ω_1 and a reduced potential φ on Ω_2, related to the magnetic field by (3.51) and (3.47). The governing differential equations are thus Poisson's equations (3.52) and (3.50) for ϕ on Ω_1 and φ on Ω_2 respectively, in which $\mathbf{H}_c$ vanishes since there are no permanent magnets.

To set boundary conditions, we partition Γ in two (assumed connected) parts Γ_N and Γ_D such that $\Gamma_N \cup \Gamma_D = \Gamma$, depending on where normal and tangential components of the magnetic field are known. We introduce the partial boundaries $\Gamma_{N,1} = \Gamma_N \cap \partial\Omega_1$, $\Gamma_{D,1} = \Gamma_D \cap \partial\Omega_1$ and $\Gamma_{N,2} = \Gamma_N \cap \partial\Omega_2$, $\Gamma_{D,2} = \Gamma_D \cap \partial\Omega_2$ on which (3.61)-(3.62) and (3.59)-(3.60) are respectively assigned. Considering in Γ_I the interface conditions (3.53) and (3.56), we have finally the following differential boundary value problem on Ω:

$$\begin{cases} -\nabla \cdot (\mu_1 \nabla \phi) = 0 & \text{on } \Omega_1 \\ -\nabla \cdot (\mu_2 \nabla \varphi) = -\nabla \cdot (\mu_2 \mathbf{H}_s) & \text{on } \Omega_2 \\ \phi(\mathbf{r}) = \varphi(\mathbf{r}) - \int_{\mathbf{r}_0}^{\mathbf{r}} \mathbf{H}_s \cdot d\mathbf{r}, \quad \phi(\mathbf{r}_0) = \varphi(\mathbf{r}_0) & \text{on } \Gamma_I \\ \mu_1 \nabla \phi \cdot \mathbf{n}_1 + \mu_2 \nabla \varphi \cdot \mathbf{n}_2 = \mu_2 \mathbf{H}_s \cdot \mathbf{n}_2 & \text{on } \Gamma_I \\ \phi(\mathbf{r}) = \int_{\mathbf{r}_A}^{\mathbf{r}_0} \mathbf{H}_s \cdot d\mathbf{r} & \text{on } \Gamma_{D,1} \\ \varphi(\mathbf{r}) = \int_{\mathbf{r}_A}^{\mathbf{r}} \mathbf{H}_s \cdot d\mathbf{r}, \quad \varphi(\mathbf{r}_A) = 0 & \text{on } \Gamma_{D,2} \\ \nabla \phi \cdot \mathbf{n}_1 = 0 & \text{on } \Gamma_{N,1} \\ \nabla \varphi \cdot \mathbf{n}_2 = \mathbf{H}_s \cdot \mathbf{n}_2 & \text{on } \Gamma_{N,2} \end{cases} \tag{4.20}$$

in the unknowns ϕ and φ on their respective domains Ω_1 and Ω_2, where $\mathbf{r}_0 \in \Gamma_I$ and $\mathbf{r}_A \in \Gamma_{D,2}$ are fixed arbitrarily. Figure 2 shows a schematic 2D version of the model domain. In (4.20) $\mathbf{H}_s$ represents the source magnetic field intensity due to $\mathbf{J}_s$, which can be computed using the Biot-Savart law (3.48), as described in [27].

Since problem (4.20) belongs to the class (4.1) with data f, d, p, q and u_D related to $\mathbf{H}_s$ by differentiation or line integration, we can therefore use the weak formulation (4.3) for a finite element solution by Galerkin discretization, according to the discrete form (4.19).

Once the potentials ϕ and φ have been computed by solution of model (4.20), and consequently the fields $\mathbf{H}$ and $\mathbf{B}$ are known, global quantities of physical interest can be then estimated, for example the *magnetic energy*. Given a material domain $\mathcal{D} \subseteq R^3$, assuming that $\mathbf{B}$ is linearly related to $\mathbf{H}$, the total magnetic energy stored in $\mathcal{D}$ due to $\mathbf{H}$ is

$$W = \frac{1}{2} \int_{\mathcal{D}} \mathbf{B} \cdot \mathbf{H} \, d\mathbf{x} = \frac{1}{2} \int_{\mathcal{D}} \mu H^2 \, d\mathbf{x}. \tag{4.21}$$

In Chapter 7, model (4.20) will be applied to some test cases and magnetic energies on material domains will be the reference global quantities computed from our FEM solution, in order to compare their values with the ones estimated by other finite element methods.

5 Error estimation and adaptivity

5.1 Types of error

Broadly speaking, differential models can be written in the general form $A(u) = g$, where A is a *differential operator*, g represents *data* and u is the *solution*. In the representation of a physical problem by a *computable* mathematical form we introduce, however, perturbations and approximations. Generally, the operator A is modelled by $\widehat{A}$ and the datum g is approximated by $\widehat{g}$. Therefore, if $\widehat{u}$ is the exact solution of the approximated model $\widehat{A}(\widehat{u}) = \widehat{g}$ the difference $e_{\mathcal{M}} = u - \widehat{u}$ represents what we can call the *modelling error*. Then, depending on the discretization method and the computation algorithm, we also have to take into consideration the *computational error* $e_{\mathcal{C}} = \widehat{u} - U$ where U is the approximated solution of $\widehat{A}(\widehat{u}) = \widehat{g}$. The total error is thus the sum of both the modelling and computational errors:

$$e = u - U = (u - \widehat{u}) + (\widehat{u} + U) = e_{\mathcal{M}} + e_{\mathcal{C}}. \tag{5.1}$$

In this work, we intend to investigate the computational error, dominant part of the error when the computational model $\widehat{A}(\widehat{u}) = \widehat{g}$ is a "sufficiently" good approximation of the exact model $A(u) = g$. Here, the approximated solution U is intended to be the finite element solution u_h of the variational form (4.3), obtained by solving the discrete form (4.19). A future task for a global error analysis will be then to investigate other error contributions. In our model, which involves several steps of modelling and computation, the sources of "perturbation" arise in fact in modelling of data at more levels (computation of $\mathbf{H}_s$, discretization of $\mathbf{H}_s \cdot \mathbf{n}$ for the Neumann conditions, quadrature of $\int \mathbf{H}_s \cdot d\mathbf{r}$ for the Dirichlet conditions) as well as numerical computation (Galerkin finite element discretization, linear system solution).

Consider now the *finite element error*

$$e = u - u_h, \tag{5.2}$$

where u is the exact solution of a certain model and u_h is the finite element solution. Error estimates of (5.2) provide a measure of the accuracy and stability of the finite element solution. They can be given in two forms, as *a priori* and *a posteriori estimates*.

A priori error estimates for (5.2) are expressed in terms of the exact solution, so that they can give information about regularity properties of the exact solution and the order of convergence of the finite element method. Differently from the former, a posteriori estimates are expressed in terms of data, mesh size and finite element solution, i.e. they are defined by quantities that are all *computable*. The latter turn out to be useful to suggest operative criteria to improve the solution accuracy by successive steps of finite element calculation in a *feed-back* process resorting to known or previously computed information.

In this case, no a priori information of the exact solution are required.

In an *adaptive* finite element method, a posteriori error estimates are used inside a computational procedure that constructs a finite element discretization for a given problem according to two basic objectives [21]:

(a) the error of the approximate solution lies within a given tolerance;
(b) the finite element solution is obtained by a (nearly) minimal number of degrees of freedom.

By condition (a) we require that the method is *reliable*, and by condition (b) that it is also *efficient*.

The basic idea behind an adaptive finite element algorithm is the following. If a global a posteriori error estimate is lower than a given tolerance, the finite element solution is considered accurate (and the algorithm stops). Otherwise, local error indicators are computed on mesh entities (elements, nodes, or edges/faces) for a "local" improvement of the solution accuracy by refinement/correction of selected entities on which the error indicator results large. Regarding this, we can distinguish essentially three refinement approaches:

- *h-refinement*, decrease of the element size;
- *p-refinement*, increase of the order in the polynomial representation of the solution;
- *r-refinement*, movement/correction of node positions.

Once the refinement procedure has been performed on the mesh, a successive and more accurate finite element solution is then computed using the new definition of the degrees of freedom. In the present paper we deal with h-refinement techniques and in Section 5.3 we will describe how they have been applied to finite element meshes.

Many authors (I. Babuska, W.C. Rheimboldt, R.E. Bank, A. Weiser, O.C. Zienkiewicz, C. Johnson, R. Verfurth, J.E. Flaherty, and some others) have studied adaptive finite element methods according to a posteriori error indicators estimated by different criteria. See references [3, 5, 7, 18, 20, 21, 31, 32, 33, 49] and, for a more complete list, the ones quoted in [18, 23, 49].

Among the ones above mentioned, the first a posteriori error estimator has been suggested by Babuska and Bank in the 80's. In that case the error was computed from the solution of "perturbed" local variational problems, where residual quantities appeared as data for the error model. This idea has been used recently for static electromagnetic models in [2, 25], and for eddy current problems in [23]. Differently from Babuska's, in Johnson's approach error estimates are provided as upper bounds of the error in proper norms ($\| e \|_{L_2}$, $\| e \|_{H_1}$, $\| e \|_{\mathcal{E}}$, etc.), related to residual quantities occurring at the interior and the boundary of the elements, up to proper constants. Basically these error estimates are obtained by using the orthogonality properties of the Galerkin method together with standard finite element interpolation estimates, and they require an estimation of stability factors, which can be obtained by solving *dual problems* associated to the initial one.

According to these guidelines, in the next section we extend some arguments proposed in [18, 21] for classical Poisson problems, to prove some a posteriori estimates of (5.2) for the finite element solution of model (4.20). Aiming at this, we consider the abstract framework presented in Chapter 4.

5.2 A posteriori error estimation

Under the hypotheses and notations introduced in Section 4.2, we have seen that the model problem (4.1) can always be associated to a variational form (4.10) with the bilinear form a and the linear functional b defined in (4.8) and (4.11), which is equivalent to (4.3). Let therefore u be the exact solution of (4.3), obtained from the solution $\tilde{u}$ of (4.10) and relation (4.7). Similarly, let u_h be the discrete solution, computed from the Galerkin finite element solution $\tilde{u}_h$ of (4.19) and the definition

$$u_h = \tilde{u}_h + \tilde{u}_{D,h}, \tag{5.3}$$

where $\tilde{u}_{D,h}$ is the projection of $\tilde{u}_D$ in the finite-dimensional space $V^r_{h,\Gamma_I} \subseteq H^1(\Omega_1, \Omega_2)$ of functions that are continuous on Ω_1 and Ω_2, piecewise defined polynomials of order r over each element in T_h. As regards u and u_h in the original models, we use the same bilinear form a as defined in (4.8), and introduce a functional g obtained from b in (4.11) such that

$$g(v) = (f, v)_\Omega + <q, v>_{\Gamma_N} + <p, v>_{\Gamma_I}, \quad \forall v \in H^1_{0,\Gamma_D}(\Omega). \tag{5.4}$$

By construction, we know that u satisfies (4.3), i.e.

$$a(u, v) = g(v), \qquad \forall v \in H^1_{0,\Gamma_D}(\Omega), \tag{5.5}$$

together with the non-homogeneous Dirichlet conditions on Γ_D and Γ_I, and u_h satisfies the discrete form

$$a(u_h, v_h) = g(v_h), \qquad \forall v_h \in V^r_h. \tag{5.6}$$

Under these premises, from (5.5) and (5.6) it follows:

Proposition. *The finite element error* (5.2) *satisfies the "orthogonality" property*

$$a(e, v_h) = 0, \qquad \forall v_h \in V^r_h. \tag{5.7}$$

In Ω we now introduce the following *residual*

$$r = -\nabla \cdot (\alpha \nabla u) - f, \tag{5.8}$$

associated to the functional

$$< r, v >= a(u_h, v) - (f, v)_\Omega - < q, v >_{\Gamma_N} - < p, v >_{\Gamma_I} \tag{5.9}$$

for each $v \in H^1_{0,\Gamma_D}(\Omega)$. Then

Lemma. *For all $v \in H^1_{0,\Gamma_D}(\Omega)$, $v_h \in V_h^r$, it holds:*

$$\begin{aligned} &< r, v >= -a(e, v), \\ &< r, v_h >= 0, \\ &< r, v >=< r, v - v_h > . \end{aligned} \tag{5.10}$$

Proof. The first one follows immediately from the linearity of a, the second one from (5.6) and the third one as a corollary, due to the linearity of $< r, \cdot >$.

Given the triangulation $T_h = \{\tau\}$, let $\mathcal{F}$ be the set of faces of all elements $\tau \in T_h$. In the following, for any face $f \in \mathcal{F}$ between a tetrahedron τ_f^+ and its adjacent τ_f^-, and any $\psi \in L^2(\overline{\tau_f^+} \cup \overline{\tau_f^-})$, we denote by ψ_f^+ and ψ_f^- the limit values of ψ on f from the two sides of τ_f^+ and τ_f^-, respectively, and by $[\psi]_f$ the jump of ψ across f in the direction of the unit vector $\mathbf{n}$ normal to f, defined by

$$\begin{aligned} &\psi_f^+ = \lim_{t \to 0^+} \psi(\mathbf{x} + t\mathbf{n}), \quad \psi_f^- = \lim_{t \to 0^-} \psi(\mathbf{x} - t\mathbf{n}), \quad \forall \mathbf{x} \in f, \\ &[\psi]_f = \psi_f^+ - \psi_f^- . \end{aligned} \tag{5.11}$$

Now it is possible to demonstrate the following a posteriori error estimate for (5.2):

Theorem 5.1. *The energy norm of the Galerkin finite element error* (5.2) *in the variational problem* (4.3) *satisfies the following property: there exists a constant $C > 0$ for which*

$$\| e \|_{\mathcal{E},\Omega} \le C \| \tilde{h} R \|_{L_2(\Omega)}, \tag{5.12}$$

where $\tilde{h} = \tilde{h}(x)$ and $R = R(x)$ are the functions piecewise defined on each element τ such that

$$\begin{aligned} &\tilde{h}\,|_\tau = h_\tau \\ &R\,|_\tau = |-\nabla \cdot (\alpha \nabla u_h) - f\,| + h_\tau^{-1/2} \mathrm{Meas}(\tau)^{-1/2}\, S_\tau, \end{aligned} \tag{5.13}$$

with $h_\tau = \mathrm{diam}(\tau)$, and

$$
\begin{aligned}
S_\tau = &\parallel \eta_\tau([\alpha\nabla u_h\cdot\mathbf{n}]-p)\parallel_{L_2(\partial\tau\cap\Gamma_I)} \\
&+\parallel \eta_\tau[\alpha\nabla u_h\cdot\mathbf{n}]\parallel_{L_2(\partial\tau\setminus(\Gamma\cup\Gamma_I))}+\parallel \alpha\nabla u_h\cdot\mathbf{n}-q\parallel_{L_2(\partial\tau\cap\Gamma_N)},
\end{aligned}
\tag{5.14}
$$

where $\{\eta_\tau\}_{\tau\in T_h}$ is a family of positive real numbers chosen in such a way that $0<\eta_\tau<1$ for all $\tau\in T_h$, with $\eta_{\tau_i}+\eta_{\tau_j}=1$ if τ_i and τ_j are adjacent.

Proof. The demonstration is based on the elementwise decomposition of the integrals defining a and g by the triangulation T_h. First, we write

$$
<p,v>_{\Gamma_I}=\sum_{f\in\mathcal{F}}\int_{f\cap\Gamma_I} pv\,d\mathcal{S}, \tag{5.15}
$$

define

$$
a_\tau(u,v)=\int_\tau \alpha\nabla u\cdot\nabla v\,d\mathbf{x},\quad \forall v\in H^1_{0,\Gamma_D}(\Omega), \tag{5.16}
$$

and consider the set decomposition

$$
\partial\tau=(\partial\tau\cap\Gamma_D)\cup(\partial\tau\cap\Gamma_N)\cup(\partial\tau\cap\Gamma_I)\cup(\partial\tau\setminus(\Gamma\cup\Gamma_I)). \tag{5.17}
$$

Then, we have

$$
\begin{aligned}
<r,v> &= \sum_{\tau\in T_h}\big(a_\tau(u_h,v)-(f,v)_\tau-<q,v>_{\partial\tau\cap\Gamma_N}\big)-\sum_{f\in\mathcal{F}}<p,v>_{f\cap\Gamma_I}\\
&=\sum_{\tau\in T_h}\big((-\nabla\cdot(\alpha\nabla u_h)-f,v)_\tau+<\alpha\partial u_h/\partial n-q,v>_{\partial\tau\cap\Gamma_N}\\
&\quad+<\alpha\partial u_h/\partial n,v>_{\partial\tau\setminus\Gamma}\big)-\sum_{f\in\mathcal{F}}<p,v>_{f\cap\Gamma_I}\\
&=\sum_{\tau\in T_h}\big((-\nabla\cdot(\alpha\nabla u_h)-f,v)_\tau+<\alpha\nabla u_h\cdot\mathbf{n}-q,v>_{\partial\tau\cap\Gamma_N}\big)\\
&\quad+\sum_{f\in\mathcal{F}}\big(<[\alpha\nabla u_h\cdot\mathbf{n}]_f-p,v>_{f\cap\Gamma_I}+<[\alpha\nabla u_h\cdot\mathbf{n}]_f,v>_{f\setminus(\Gamma\cup\Gamma_I)}\big)\\
&=\sum_{\tau\in T_h}\big((-\nabla\cdot(\alpha\nabla u_h)-f,v)_\tau+<\alpha\nabla u_h\cdot\mathbf{n}-q,v>_{\partial\tau\cap\Gamma_N}\\
&\quad+<\eta_\tau([\alpha\nabla u_h\cdot\mathbf{n}]-p),v>_{\partial\tau\cap\Gamma_I}+<\eta_\tau[\alpha\nabla u_h\cdot\mathbf{n}],v>_{\partial\tau\setminus(\Gamma\cup\Gamma_I)}\big),
\end{aligned}
\tag{5.18}
$$

where $\{\eta_\tau\}_{\tau\in T_h}$ is a set of weights chosen so that $0<\eta_\tau<1$ for all $\tau\in T_h$, and $\eta_{\tau_i}+\eta_{\tau_j}=1$ if τ_i and τ_j are adjacent. Considering now the third relation in (5.10), the Cauchy-Schwartz inequality and the monotony property for integrals, we obtain

$$
\begin{aligned}
|\langle r, v\rangle| \leq \sum_{\tau\in T_h} \Big(& \| -\nabla\cdot(\alpha\nabla u_h) - f \,\|_{L_2(\tau)} \| v - v_h \|_{L_2(\tau)} \\
& + \| \alpha\nabla u_h\cdot\mathbf{n} - q \|_{L_2(\partial\tau\cap\Gamma_N)} \| v - v_h \|_{L_2(\partial\tau)} \\
& + \| \eta_\tau([\alpha\nabla u_h\cdot\mathbf{n}] - p) \|_{L_2(\partial\tau\cap\Gamma_I)} \| v - v_h \|_{L_2(\partial\tau)} \\
& + \| \eta_\tau[\alpha\nabla u_h\cdot\mathbf{n}] \|_{L_2(\partial\tau\setminus(\Gamma\cup\Gamma_I))} \| v - v_h \|_{L_2(\partial\tau)} \Big).
\end{aligned}
\tag{5.19}
$$

Two fundamental inequalities have then to be used on elements τ and their boundary (see [18, 43]). The first one is a local version of the *trace inequality* (2.16): given a function $\omega \in H^1(\tau)$ there exists a constant $C_{\tau,0} > 0$ such that

$$
\| \omega \|_{L_2(\partial\tau)} \leq C_{\tau,0}\big(h_\tau^{-1/2} \| \omega \|_{L_2(\tau)} + h_\tau^{1/2} \| \nabla\omega \|_{L_2(\tau)} \big). \tag{5.20}
$$

The second one is a classical result from interpolation theory: denoted by Ω_τ the union of the closure of elements adjacent to any element τ, for any function $\omega \in H^1(\Omega_\tau)$ there exists a constant $C_{\tau,1} > 0$ for which

$$
\| D^{(m)}(\omega - \pi_h\omega) \|_{L_2(\tau)} \leq C_{\tau,1}\, h_\tau^{l-m} \| D^{(l)}\omega \|_{L_2(\Omega_\tau)}, \tag{5.21}
$$

for $m = 0, 1,\ l = 1, 2$, where $\pi_h\omega$ is the nodal interpolant of ω at nodes of Ω_τ, with $D^{(0)}\omega = \omega$ and $D^{(1)}\omega = \nabla\omega$. In particular, it follows

$$
\begin{aligned}
& \| v - \pi_h v \|_{L_2(\tau)} \leq C_{\tau,1} h_\tau \| \nabla v \|_{L_2(\Omega_\tau)} \\
& \| \nabla(v - \pi_h v) \|_{L_2(\tau)} \leq C_{\tau,1} \| \nabla v \|_{L_2(\Omega_\tau)},
\end{aligned}
\tag{5.22}
$$

hence

$$
\| v - \pi_h v \|_{L_2(\partial\tau)} \leq C_{\tau,2}\, h_\tau^{1/2} \| \nabla v \|_{L_2(\Omega_\tau)} \tag{5.23}
$$

with $C_{\tau,2} = 2\, C_{\tau,0} C_{\tau,1}$. We substitute the first inequality of (5.22) and (5.23) in (5.19), and resume all the constants to obtain

$$
\begin{aligned}
|\langle r, v\rangle| \leq C^{(0)} \sum_{\tau\in T_h} \Big(& h_\tau \| -\nabla\cdot(\alpha\nabla u_h) - f \|_{L_2(\tau)} + h_\tau^{1/2} \big(\| \eta_\tau[\alpha\nabla u_h\cdot\mathbf{n}] \|_{L_2(\partial\tau\setminus(\Gamma\cup\Gamma_I))} \\
& + \| \eta_\tau([\alpha\nabla u_h\cdot\mathbf{n}] - p) \|_{L_2(\partial\tau\cap\Gamma_I)} + \| \alpha\nabla u_h\cdot\mathbf{n} - q \|_{L_2(\partial\tau\cap\Gamma_N)} \big) \Big) \| \nabla v \|_{L_2(\Omega_\tau)}
\end{aligned}
\tag{5.24}
$$

for a constant $C^{(0)} > 0$. Then, we consider the monotony property for the integration domains $\Omega_\tau \subseteq \Omega$, the upper bound

$$
\sum_{i=1}^n a_i \leq \kappa_n \Big(\sum_{i=1}^n a_i^2 \Big)^{1/2}, \quad \forall a_i \geq 0, \quad i = 1, 2, \ldots, n, \tag{5.25}
$$

which holds for some constants $\kappa_n > 0$, as well as the bounds $a^2 + b^2 \leq (a+b)^2 \leq 2a^2 + 2b^2$ for all a, $b \geq 0$. After some rearrangement, by introduction of the global notations (5.13) and (5.14), we get

$$|<r, v>| \leq C^{(1)} \| \tilde{h} R \|_{L_2(\Omega)} \| \nabla v \|_{L_2(\Omega)} \tag{5.26}$$

for the constant $C^{(1)} = \sqrt{2}\, \kappa_n C^{(0)}$. Then, we choose $v = e$ and use the equality

$$|<r, e>| = \| e \|^2_{\mathcal{E},\Omega}, \tag{5.27}$$

obtained from the first equation in (5.10). To conclude, we consider the equivalence between norms $\| e \|_{\mathcal{E},\Omega}$ and $\| \nabla e \|_{L_2(\Omega)}$. In particular, from

$$\alpha_{min} \| \nabla e \|^2_{L_2(\Omega)} \leq \| e \|^2_{\mathcal{E},\Omega} \tag{5.28}$$

we get the upper bound in L_2-norm

$$\| \nabla e \|_{L_2(\Omega)} \leq \tilde{C} \; \| \tilde{h} R \|_{L_2(\Omega)} \tag{5.29}$$

with $\tilde{C} = C^{(1)}/\alpha_{min}$. On the other hand, from

$$\alpha_{max} \| \nabla e \|^2_{L_2(\Omega)} \geq \| e \|^2_{\mathcal{E},\Omega} \tag{5.30}$$

relation (5.12) finally holds, by choosing $C = C^{(1)} \sqrt{\alpha_{max}}/\alpha_{min}$. *Q.E.D.*

The above estimation on Ω shows that the energy norm of the finite element error depends on the residual at the interior of elements, in a proportional way to the mesh size h_τ, as well as the residual at the inter-element jump of the normal derivative of the solution, in a proportional way to $h_\tau^{1/2}$.

For the numerical computation of (5.12) two important aspects have to be considered. The first one concerns the weights η_τ appearing in the pairwise contributions across element faces. Although an infinite number of values can be assigned to them, it is convenient to define them in such a way that the corresponding terms in the upper bound (5.12) become as small as possible. The simplest choice is to take $\eta_\tau = 1/2$, i.e. to consider an *equidistribution* of the error contribution due to jumps of the normal derivative. A better choice, however, is to define a different weight from element to element, taking into account the geometry of the problem domain, the possible discontinuity of the diffusion coefficient α across elements, as well as local behaviours of the finite element solution (e.g. gradients, etc.). Regarding this, a possible non-uniform definition of the weights η_τ is suggested in the following Theorem 5.2.

The second (crucial) aspect is to provide an appropriate estimation of the constants C and $\tilde{C}$. The proof of Theorem 5.1 suggests how to compute them, by their relation with the constants appearing in the trace and interpolation inequalities (5.20) and (5.21). Nevertheless, such estimates would be too large. A sharper estimation than (5.12) is rather obtained by separating the contributions of the interior residuals and the jumps of the normal derivative across the element faces with introduction of two different constants, instead of one, resorting to few modifications in the previous demonstration.

Taking into account these two practical difficulties, a finer error estimation is then suggested by modification of the global general upper bound (5.12), as follows.

Theorem 5.2. *The energy norm of the Galerkin finite element error* (5.2) *in the variational problem* (4.3) *satisfies the following property: there exist two constants* $C_1 > 0$ *and* $C_2 > 0$ *for which*

$$
\begin{aligned}
\| e \|_{\mathcal{E},\Omega}^2 &= \| \alpha^{1/2} \, \nabla(u - u_h) \|_{L_2(\Omega)}^2 \qquad (5.31)\\
&\leq \sum_{\tau \in T_h} \Big(\, C_1 \, \| \alpha^{-1/2} h_\tau (-\nabla \cdot (\alpha \nabla u_h) - f) \|_{L_2(\tau)}^2 \\
&\qquad + C_2 \Big(\sum_{f \in (\partial\tau \setminus (\Gamma \cup \Gamma_I))} \| (\alpha^+ + \alpha^-)^{-1/2} h_f^{1/2} [\alpha \nabla u_h \cdot \mathbf{n}]_f \|_{L_2(f)}^2 \\
&\qquad + \sum_{f \in (\partial\tau \cap \Gamma_I)} \| (\alpha^+ + \alpha^-)^{-1/2} h_f^{1/2} ([\alpha \nabla u_h \cdot \mathbf{n}]_f - p) \|_{L_2(f)}^2 \\
&\qquad + \sum_{f \in (\partial\tau \cap \Gamma_N)} \| (\alpha^{-1/2} h_f^{1/2} (\alpha \nabla u_h \cdot \mathbf{n} - q) \|_{L_2(f)}^2 \Big) \Big),
\end{aligned}
$$

where h_τ *and* h_f *denote the element and face sizes, defined by* $h_\tau = \mathrm{diam}(\tau)$ *and* $h_f = \mathrm{diam}(f)$ *for each face* f *in* τ, *for* $\tau \in T_h$, *and where* α^+ *and* α^- *denote the limit values of* α *at each face* f *of* τ *from its interior and exterior respectively, according to notation* (5.11).

Proof. The demonstration is similar to the one of Theorem 5.1. The fundamental difference consists in the specification of the weights η_τ and in a different definition of the constant factors. Again, we compute $< r, v >$. In the last right hand side of equation (5.18) we can divide and multiply by $\alpha^{1/2}$ the addends referred to τ and $\partial\tau \cap \Gamma_N$, and multiply and divide by $h_\tau^{1/2}$ the addends referred to $\partial\tau \cap \Gamma_N$, $\partial\tau \cap \Gamma_I$ and $\partial\tau \setminus (\Gamma \cup \Gamma_I)$. Then, we define the weights η_τ introduced in Theorem 5.1 so that

$$
\eta_\tau|_f = \frac{\alpha^+}{\alpha^+ + \alpha^-}, \qquad (5.32)
$$

for each face f of element τ. If we split in two factors the contributions of η_τ by the substitution

$$\eta_\tau = \eta_\tau^* \sqrt{\alpha^+} \tag{5.33}$$

with $\eta_\tau^*|_f = \sqrt{\alpha^+}/(\alpha^+ + \alpha^-)$, equation (5.19) takes the modified form

$$\begin{aligned}
|{<}r, v{>}| \leq \sum_{\tau \in T_h} \Big(& \| \alpha^{1/2}(v - v_h) \|_{L_2(\tau)} \, \| \alpha^{-1/2}(-\nabla \cdot (\alpha \nabla u_h) - f) \|_{L_2(\tau)} \\
& + \| \alpha^{1/2} h_\tau^{-1/2}(v - v_h) \|_{L_2(\partial\tau)} \, \big(\| \alpha^{-1/2} h_\tau^{1/2}(\alpha \nabla u_h \cdot \mathbf{n} - q) \|_{L_2(\partial\tau \cap \Gamma_N)} \\
& + \| \eta_\tau^* h_\tau^{1/2}([\alpha \nabla u_h \cdot \mathbf{n}] - p) \|_{L_2(\partial\tau \cap \Gamma_I)} + \| \eta_\tau^* h_\tau^{1/2} [\alpha \nabla u_h \cdot \mathbf{n}] \|_{L_2(\partial\tau \setminus (\Gamma \cup \Gamma_I))} \big) \Big).
\end{aligned} \tag{5.34}$$

From (5.22) and (5.23) we obtain the inequalities

$$\begin{aligned}
\| \alpha^{1/2}(v - \pi_h v) \|_{L_2(\tau)} &\leq \tilde{C}_{\tau,1} h_\tau \| \nabla v \|_{L_2(\Omega_\tau)} \\
\| \alpha^{1/2} h_\tau^{-1/2}(v - \pi_h v) \|_{L_2(\partial\tau)} &\leq \tilde{C}_{\tau,2} \| \nabla v \|_{L_2(\Omega_\tau)},
\end{aligned} \tag{5.35}$$

where $\tilde{C}_{\tau,1} = C_{\tau,1} \alpha_{\max,\tau}^{1/2}$ and $\tilde{C}_{\tau,2} = C_{\tau,2} \alpha_{\max,\tau}^{1/2}$, with $\alpha_{\max,\tau}$ maximum diffusion value on $\overline{\tau}$. We now consider the upper bound

$$\frac{\sqrt{\alpha^+}}{\alpha^+ + \alpha^-} < \frac{1}{\sqrt{\alpha^+ + \alpha^-}}, \tag{5.36}$$

and split the boundary contributions on each element along the single faces. If we denote by $h_f = \mathrm{diam}(f)$ the size of each face f, for any tetrahedron $\tau \in T_h$ there exists a constant $\kappa_\tau > 0$ depending on the geometry of the tetrahedron such that $h_\tau \leq \kappa_\tau h_f$ for any face f of τ. Thus, summarizing all elemental constants $\tilde{C}_{\tau,1}$ and κ_τ in a global $\tilde{C}_1$, as well as $\tilde{C}_{\tau,2}$ and κ_τ in a $\tilde{C}_2$, we obtain

$$\begin{aligned}
|{<}r, v{>}| \leq \sum_{\tau \in T_h} \Big(& \tilde{C}_1 \, \| \alpha^{-1/2} h_\tau (-\nabla \cdot (\alpha \nabla u_h) - f) \|_{L_2(\tau)} \\
& + \tilde{C}_2 \big(\sum_{f \in (\partial\tau \setminus (\Gamma \cup \Gamma_I))} \| (\alpha^+ + \alpha^-)^{-1/2} h_f^{1/2} [\alpha \nabla u_h \cdot \mathbf{n}]_f \|_{L_2(f)} \\
& + \sum_{f \in (\partial\tau \cap \Gamma_I)} \| (\alpha^+ + \alpha^-)^{-1/2} h_f^{1/2} ([\alpha \nabla u_h \cdot \mathbf{n}]_f - p) \|_{L_2(f)} \\
& + \sum_{f \in (\partial\tau \cap \Gamma_N)} \| (\alpha^{-1/2} h_f^{1/2} (\alpha \nabla u_h \cdot \mathbf{n} - q) \|_{L_2(f)} \big) \Big) \| \nabla v \|_{L_2(\Omega_\tau)},
\end{aligned} \tag{5.37}$$

as a modification of (5.24). Again, we choose $v = e$, apply equality (5.27) and consider bounds (5.28) and (5.30). Taking here $\| e \|_{\mathcal{E},\Omega}^2$ instead of $\| e \|_{\mathcal{E},\Omega}$ and using inequality (5.25), we finally obtain estimation (5.31) for suitable constants $C_1 > 0$ and $C_2 > 0$ related to $\tilde{C}_1^2$ and $\tilde{C}_2^2$ respectively. *Q.E.D.*

Giving a more detailed information than the general bound (5.12), estimation (5.31) shows that the elemental contribution of the error due to the interior residual is inversely proportional to $\alpha^{1/2}$ and proportional to the element size, while the local contributions on the element boundary take into account the discontinuity of diffusion across the faces, inversely proportional to $(\alpha^+ + \alpha^-)^{1/2}$ and proportional to the square root of the face sizes.

In the particular case without any interfaces, (5.31) coincides with the error estimate introduced by X. Cai and K. Samuelsson in [13]. This represents the indicator that has been used in the present work for adaptive refinement purposes, since a numerical estimation of the constants C_1 and C_2 has already been derived in [13] both in the 2D and 3D case. These estimates result in fact sharper than the large constants obtained from the trace and interpolation inequalities. The suggested values are $C_1 = 0.1$, $C_2 = 0.15$ for triangles and $C_1 = 0.07$, $C_2 = 0.55$ for tetrahedra (used here). In the next section we will describe the algorithm of adaptive h-refinement applied to our model.

To conclude, alternative approaches of a posteriori error estimation could be proposed, depending on which quantity is considered for measuring the error on it. Here, we have focused mainly on the pure error of the potential, in order to evaluate directly the accuracy of the Galerkin finite element solution of the discrete form (4.19) associated to model (4.1). An alternative criterion could be to estimate the error on the "energy" defined by

$$\mathcal{E} = \int_{\mathcal{D}} |\nabla u|^2 \, d\mathbf{x} - \int |\nabla u_h|^2 \, d\mathbf{x} \tag{5.38}$$

or, better in our case with diffusion $\alpha = \mu$, by

$$\mathcal{E}_\mu = \int_{\mathcal{D}} \mu \, |\nabla u|^2 \, d\mathbf{x} - \int \mu \, |\nabla u_h|^2 \, d\mathbf{x}, \tag{5.39}$$

for certain domains $\mathcal{D} \subseteq \mathcal{R}^3$ contained in Ω or Ω_i, $i = 1, 2$, related to physical materials of the model. In the magnetostatic problem (4.20), in fact, the latter definition is related to a "physical" quantity, i.e. the magnetic energy (4.21), by means of definitions (3.47) and (3.51). This approach would be efficient for models derived by field formulations, as it has been tested in [8, 10]. As concerns scalar potential formulations, the new definition of error seems appropriate for domains where only *total* potentials are introduced, like in electrostatic models, or in magnetostatic models having permanent magnets but *not* source currents. In our case, the error $\mathcal{E}_\mu$ does not coincide completely with the effective error of the physical magnetic energy because of a *double* potential formulation that has recourse necessarily to a *reduced* potential φ in a part of the domain containing currents. In this case, in fact, also the contribution of the source field $\mathbf{H}_s$ has to be taken into account in the estimation of the magnetic energy.

5.3 Adaptive mesh refinement

To construct an adaptive finite element solution based on refinement of the mesh, we have to specify a criterion of selection of the mesh entities to be refined, together with a geometric technique of refinement. First, the prior requirement is that an a posteriori estimation of the finite element error has been provided in a suitable norm $\|\cdot\|$, depending on the problem and the finite element formulation. Then, as quantitative information from which to generate the adaptive procedure, we can consider:

(a) a global relative error indicator, to be measured on the overall domain;

(b) local absolute error estimates in norm, to be computed for each element of the mesh.

The global indicator (a) is computed from local data (b), once the norm of the finite element solution has been estimated. Depending on the magnitude of the local absolute error values, we then decide whether the solution is enough accurate or an adaptive refinement procedure has to be applied on the mesh entities for a successive and more accurate finite element solution on the refined mesh.

For our problem (4.20), we consider the a posteriori error estimation (5.31) in energy norm. Given a finite element triangulation T_h, we assume as local absolute error estimates each of the addends appearing at the right hand side of (5.31), in the following denoted by $\epsilon_{h,\tau}^2$ for each $\tau \in T_h$. Thus, the quantity

$$\varepsilon = \frac{\sqrt{\sum_{\tau \in T_h} \epsilon_{h,\tau}^2}}{\| u_h \|_\Omega} \tag{5.40}$$

is assumed as a definition of global relative error indicator on Ω, where u_h is the finite element solution on T_h and $\|\cdot\|_\Omega$ denotes the energy norm on Ω. Then, if (5.40) is lower than a prescribed tolerance, the finite element solution is considered "accurate" and the algorithm stops. Otherwise, an adaptive refinement procedure is called, consisting of *edge subdivision* depending on the magnitude of the local error indicators.

Formally, in order to decide *which* elements need to be refined and *how much*, i.e. how many edges in the element have to be split, we first consider the maximum local error indicator

$$\epsilon_{max}^2 = \max_{\tau \in T_h} \{\epsilon_{h,\tau}^2\}. \tag{5.41}$$

Then, fixed a value δ such that $0 < \delta < 1$, called *factor of refinement*, we set the $N+2$ levels

$$b_0 = 0; \qquad b_i = \delta^{N+1-i} \epsilon_{max}^2, \quad i = 1, 2, \ldots, N+1, \tag{5.42}$$

where N is the number of edges (e.g. $N = 6$, in case of tetrahedra). Hence, a refinement criterion can be the following:

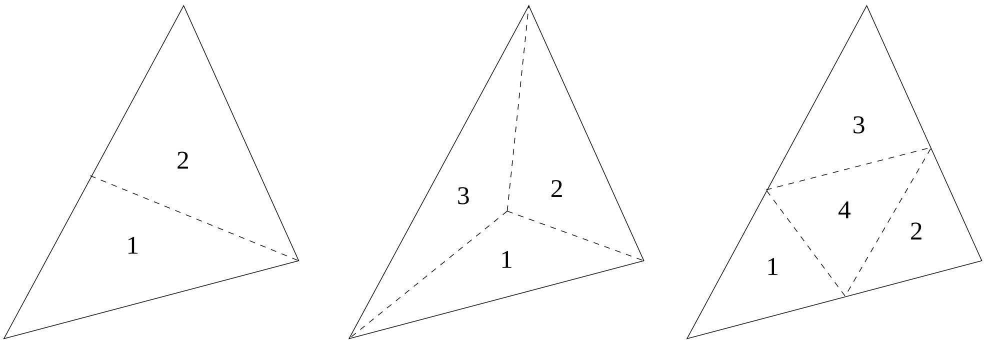

(a) edge bisection (b) centroid (c) Bank bisection

Figure 3: Classical refinement techniques for triangles

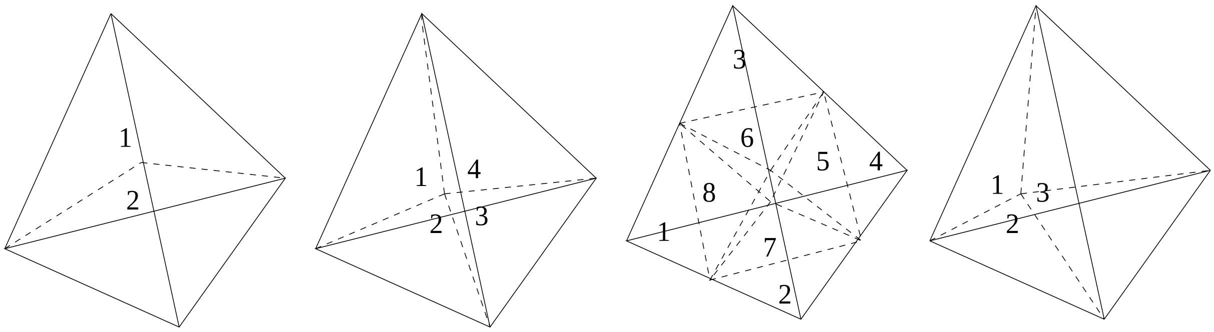

(a) edge bisection (b) centroid (c) Bank bisection (d) face bisection

Figure 4: Classical refinement techniques for tetrahedra

$\forall \tau \in T_h$:

$\quad$ *find* $j \in \{0, 1, \ldots, N\}$ *such that* $b_j < \epsilon^2_{h,\tau} \leq b_{j+1}$;

$\quad$ *split the element* τ *along* j *edges.*

In this procedure, the elements τ having $\epsilon^2_\tau \leq b_1$ are not considered for refinement.

Splitting an edge means adding a new node at the midpoint of the edge. When an element needs to be refined according to the algorithm, with subdivision of j edges, the *longest* j edges are split. When $j > 1$ more than one way can then exist to generate the derived elements from the initial one, considering the added nodes. The choice about which faces generate the derived tetrahedra (i.e. how added nodes connect old and new nodes in the original tetrahedron) is done in such a way that their shape is kept "close" to the equilateral geometry, consistently with the shape quality of old tetrahedron. This is done in order to avoid degenerations in element shapes that could not guarantee convergence of the finite element solution. In the case $j = 1$, two tetrahedra are generated from one (using the classical *edge bisection method*, as shown in Figure 4.a), while in the case $j = 6$ eight tetrahedra are generated from one (e.g. obtained by the so-called *Bank bisection method*, as shown in Figure 4.c). In the refinement of the elements, moreover, further transition elements could need to be refined in order to guarantee that the new mesh is $conformal$. The procedure of mesh refinement has been developed by K. Samuelsson at Chalmers Finite Element Center of Chalmers University of Technology. For a detailed description of Samuelsson's refinement technique, see [13, 41].

Figures 3 and 4 show several classical refinement techniques used in adaptive finite element methods for 2D and 3D triangulations. The idea of methods based on edge bisection (Figures 3.a and 4.a) and Bank bisection (Figures 3.c and 4.c), for instance, is very popular. As a short mention of alternative subdivision criteria, in the 2D case (3D, respectively) a *centroid method* (Figures 3.b., or 4.b for the 3D case) could be applied, in which three (four, respectively) elements are derived from the original one by connection of its vertices with the barycenter of the figure. For 3D meshes, moreover, the so-called *face bisection method* (Figure 4.d) could be considered, with generation of three tetrahedra from one by connection of the vertices with the barycenter of the largest face. The last two methods can, however, lead to shape degenerations and generally require techniques of mesh regularization, like *edge/face swapping*, *Delaunay triangulation*, or movement of nodes (e.g. *Laplacian smoothing*), in order to correct the shape of the new elements and make it closer to the equilateral one. See [15] for a more extended overview of these techniques, or [11, 25, 39].

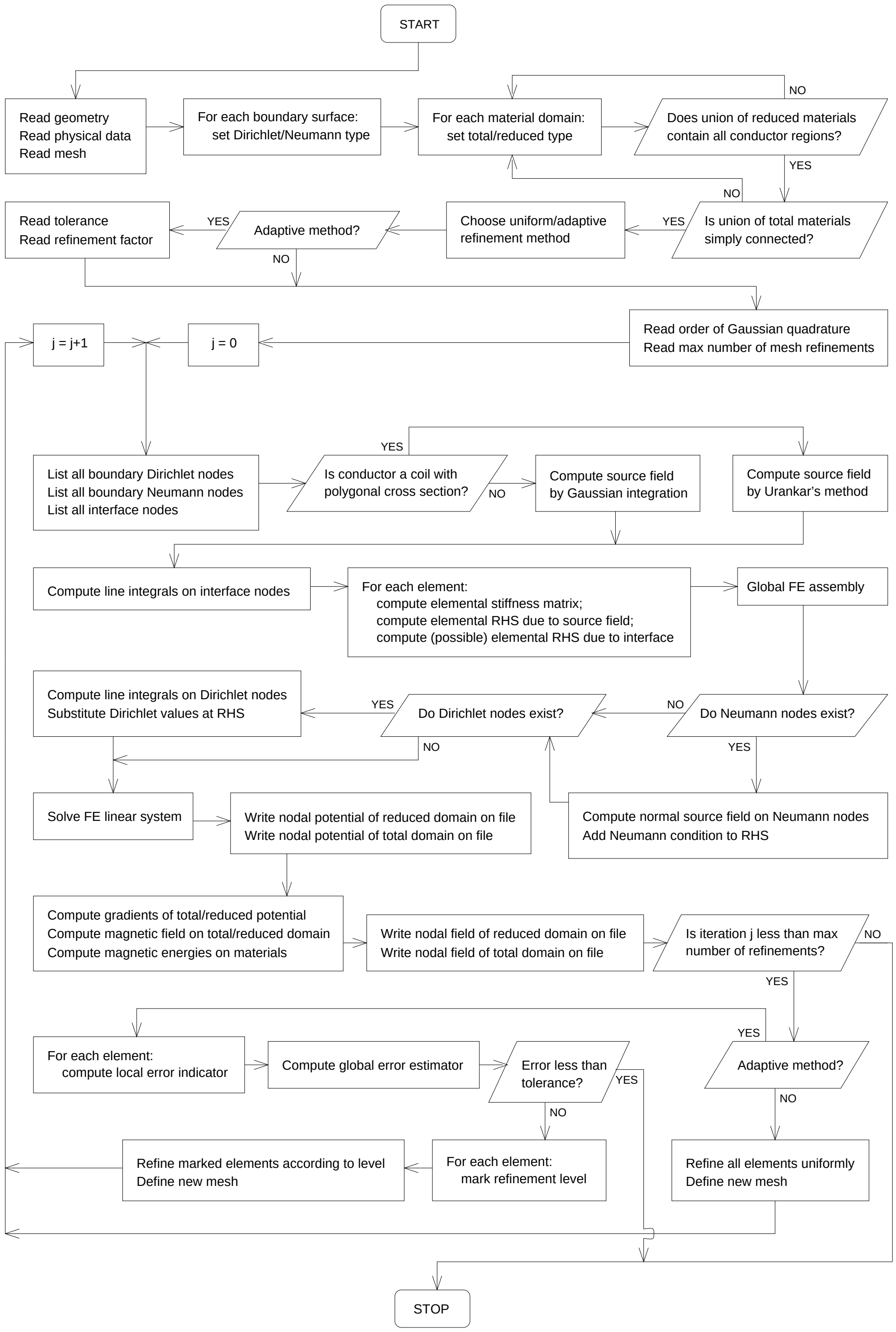

Figure 5: Flow-chart of the main algorithm

6 Implementation issues

6.1 The algorithm

The solution of the boundary value problem (4.20) has been implemented in C++ language on a Unix Sun-Solaris platform. Some advantages in the utilization of an object-oriented code for mathematical programming, especially for finite element applications, are explained in Section 6.2. The structure of the main algorithm can be represented by the flow-chart depicted in Figure 5. In this section, we briefly comment the main parts of the program.

Preprocessing

In the initial phase, a geometry, a starting (tetrahedral) mesh and physical parameters of the problem are set. The software Pro/ENGINEER has been used as a CAD tool for the construction of the domain geometry by parametric curves and surfaces in NURBS representation, exporting models in IGES format. In the preprocessing phase, typical finite element information are stored:

- *node information*: number of nodes, global node numbers and corresponding Cartesian coordinates;
- *element information*: number of elements, number of vertices per element (in case of mixed elements), global element numbers, connectivity matrix element-local nodes, type of material;
- *material information*: physical parameters associated to the materials (in our model: source current density, relative magnetic permeabilities, and possible coercive field intensity when permanent magnets exist).

Dirichlet and Neumann boundary surfaces are specified, as well as the definition of total or reduced potential on the several material domains. Mesh information are connected to the NURBS geometry.

Modelling of source data

First, the algorithm requires the estimation of quantities appearing as data in problem (4.20). In the following, we shortly describe the main modelling steps.

- *Computation of the field* $\mathbf{H}_s$ *due to* $\mathbf{J}_s$ *by estimation of Biot-Savart's integral.* Two different techniques are used, depending on shape properties of source regions, i.e. current-carrying conductors. For complex geometries, a finite volume approximation is considered, by choosing as volumes the finite elements located in the current-carrying conductors. This technique requires a triangulation that is constrained to the shape of the conductors. A composite 3D Gauss-Legendre quadrature is then applied with an appropriate order on each conductor volume. When the source regions are circular coils with rectangular cross section, a semi-analytical procedure can be used instead, based on modified Urankar's formulas [47], expressed in terms of elementary functions, Jacobian elliptic functions and elliptic integrals of the first, second and third kind [1, 12, 35]. In the last method, the numerical contribution consists of elliptic integral estimations, here performed by Carlson's algorithm [14, 36], and quadrature of one-dimensional Urankar's integrals when points are in special limit positions on which Carlson's algorithm cannot be applied. Details about these techniques are described in [27].

- *Estimation of values for the Neumann condition.* Such data are easily obtained by computation of the variational expression associated to the normal derivative of $\mathbf{H}_s$ on all the surface faces of the interface and the Neumann boundary. Nodal values are then obtained by summation of the various contributions on the surface faces to which each node belongs.
- *Estimation of values for the Dirichlet condition.* Such values are obtained by numerical estimation of line integrals $\int \mathbf{H}_s \cdot d\mathbf{r}$ on all the nodes of the surfaces at the interface and the Dirichlet boundary. The integration lines are approximated by polygonals composed of segments (edges of tetrahedra) or arcs (projected onto surfaces from the edges) on the interface or the Dirichlet boundary (called *trees*). Depending on the shape complexity of such surfaces, numerical line integration is then done by (a) 1-point quadrature rule over each edge, or (b) higher order Gauss-Legendre integration over each edge or projected arc.

In more general models, the contribution $\nabla \cdot (\mu \mathbf{H}_s)$ appearing at the right hand side of Poisson's equation has to be considered inside domains with reduced potential definition. In our assumptions, this term vanishes since materials have constant magnetic permeability and $\mathbf{H}_s$ is solenoidal.

Finite element discretization

The piecewise linear Galerkin discretization described in Section 4.3 has been applied. With respect to classical Poisson models, here we have to consider an additional step: the treatment of the condition of potential jump at the interface between domains in total potential and domains in reduced potential.

According to our double potential formulation, at the interface between regions of different potential we have to set either a *total* or *reduced* definition for the potential. Once fixed this convention, during the loop over all elements in the global FE assembly phase, nodal potential unknowns at the interface, whose elements have a definition (reduced, total) that is *opposite* to the one chosen at the interface, have to be rewritten in terms of the latter. Therefore, nodes of such interface elements have an extra contribution at the right hand side of the discrete model, derived from the associated potential jump, given by the corresponding line integral $\int \mathbf{H}_s \cdot d\mathbf{r}$ multiplied by the corresponding stiffness coefficients.

Differently from the former, no additional contribution due to potential jump has to be added at the right hand side for the elements located in regions whose potential definition is the same as the one set at the interface.

For implementation purposes, in order to reduce the error perturbation, it is suggested to choose as potential definition at the interface the same used in the domain having *larger* diffusion (i.e. higher relative magnetic permeability). In such a way, the lower diffusion coefficients of the adjacent materials give raise to lower amplification factors in the modelling error due to line integral computations.

Solution of the linear system

As a linear solver for the sparse, positive definite and symmetric FE system, the SLES module from the PETSc software package (version 2.0.28, from Argonne National Laboratory) has been utilized. PETSc is a numerical library typically used for linear algebra routines, it is designed to be particularly efficient in supporting parallel computations and includes a storage format for sparse matrices [4]. The default method of solution in the SLES kernel is a GMRES method with an incomplete ILU factorization, but many other Krylov subspace iterative methods are provided, e.g. conjugate gradient solvers, together with various preconditioning methods.

Computation of fields and magnetic energies

From the solution vector giving nodal information about potentials, a nodal representation of the field $\mathbf{H}$ is easily obtained using definitions (3.47) and (3.51), with $\mathbf{H}_s$ previously computed on the nodes in the domain with reduced potential. Since piecewise linear elements have been used, a weighted averaging of the computed potential gradients, piecewise constant, is done on neighbour elements. Magnetic energies have then been computed by numerical integration of (4.21), on each of the material domains of the model.

Error estimation and adaptive refinement

The accuracy of the finite element solution is improved by successive iterations of mesh refinement. Depending on user's initial choice, the refinement can be $uniform$, i.e. all elements are refined, or *adaptive*, i.e. only selected elements are refined.

In the adaptive approach the choice of which elements have to be refined is done according to the a posteriori error estimate in energy norm given in (5.31), computed from the finite element solution on the current mesh, data and element/face sizes. Elements of the mesh with large error indicators are then marked for refinement, according to criteria and subdivision techniques described in Section 5.3.

Since we are working with curved geometries, both in the adaptive and in the uniform

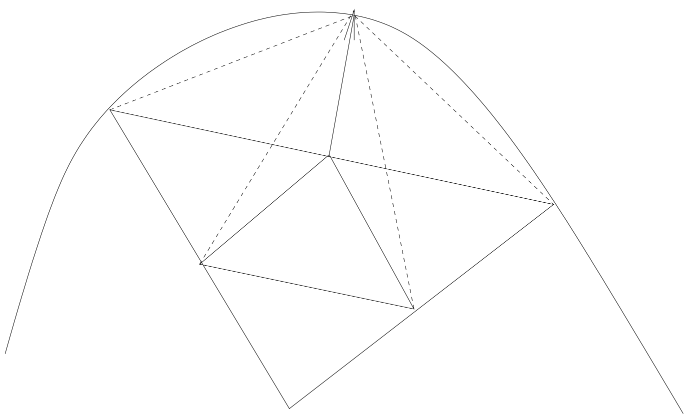

Figure 6: Projection of nodes onto curves

refinement, when elements of the old grid have faces/edges on boundaries or interfaces it is necessary to perform projections that move the new nodes onto the curved boundaries/interfaces. For the two-dimensional case, see Figure 6.

6.2 Object-oriented programming

The advantage of using an object-oriented programming language, e.g. C++, lies mainly in the possibility of working with *classes*, as complex objects having an autonomous internal representation of data and functions [6].

A consequence of this approach by classes is *modularity*. Especially when complex problems require to be handled by simpler subproblems, or need to be extended, parts of the code (modules) can be written separately by several programmers, possibly developed at a higher level of generality. These modules can be then easily grouped together inside a unique code for the purposes of the specific problem under consideration. To use an instance of an existing class inside a code, what is required to the programmer is simply to know that the class *NameClass* exists and that has a certain public or private function $.NameFunction(var1, var2, \cdots, varN)$ serving for a certain purpose. No knowledge about the internal representation of the class is required. Once declared and defined in its member data and functions as independent modulus, the class becomes a new high level type available to the programmers working on specific problems.

Moreover, in the framework of programming for mathematical purposes, the level of abstraction of object-oriented languages allows to handle equations and symbolic entities by a formal process and a code representation that appears very similar to the mathematical formalization. As examples, we can consider in its abstraction instances of a class *Equation*, as well as objects of type *Point, Line* or *Plane* for computations in Euclidean geometry, algebraic structures of type *Group, Ring*, etc., Gaussian integration methods by a class *GaussQuadrature* in which the number of nodes/weights is specified as a parameter, and so on.

6.3 Classes for finite element methods

Especially for finite element methods, the object-oriented philosophy seems to be particularly efficient when manipulating entities as differential equations in their variational form, as well as meshes, elements, basis functions, etc. Several possibilities in the choice of these classes arise. Here, we focus on the ideas that have been used in our model and its finite element solution.

Classes for equations.

First, the kernel of the model lies in the variational form of a partial or ordinary differential equation. The model (4.1), and therefore (4.20), comes from the generalized Poisson's equation $-\nabla \cdot (\alpha \nabla u) = f$ for which the simplest weak formulation is

$$\int \alpha \nabla u \cdot \nabla v d\mathbf{x} = \int \alpha(\partial u_x \partial v_x + \partial u_y \partial v_y + \partial u_z \partial v_z) d\mathbf{x} = \int f v \, d\mathbf{x} \tag{6.1}$$

in case of homogeneous Dirichlet boundary conditions, without any interfaces. For mixed boundary/interface conditions, we have seen in Section 4.2 how surface integral (3D case) or line integrals (2D case) have to be added, according to (4.3). We can therefore implement a class `PoissonEquation`, in which a function returns the elemental left hand side of (6.1) in the form

```
alpha * ( u.x()*v.x()+u.y()*u.y()+u.z()*v.z() ),
```

and a function returns the right hand side in the form

```
f * v,
```

with an evident resemblance to the above symbolic formalization. The variational equation is computed on each element of the mesh, therefore it makes sense to define an abstract superclass `Equation` to connect the specific equation (here, `PoissonEquation`) with each element and the corresponding basis functions. Observe that the member functions of `Equation` are valid for all the models, while the peculiar form of the equation is implemented in specific subclasses *EquationType* derived from it, e.g. `PoissonEquation` in our case.

Classes for grids.

The classes handling FEM meshes on arbitrary domains have been implemented at

Chalmers Finite Element Center by K. Samuelsson (see Section 5.3), and it has been possible to easily encapsulate them in the specific code written for our applications. According to Samuelsson's idea, a mesh can be seen as an instance `grid` of an abstract class `Grid` where, as an example, functions like

```
nElms=grid.getNoElms();
nNodes=grid.getNoNodes();
for (i=0; i<3; i++) x[i]=grid.getCoor(iNode,i);
matType=grid.getMaterialType(iElm);
```

return the number `nElms` of elements, the number `nNodes` of nodes, the coordinates `(x[0],x[1],x[2])` of the node whose global number is `iNode`, and the material identifier `matType` of the element `iElm`, respectively.

When a mesh has to be considered inside a hierarchy of several meshes on the same domain, as it is required for mesh refinement strategies, it is useful to derive a `GridFeHier` object as a subclass of `Grid`. The purpose of this subclass is to keep track of the relationships among entities referred to a grid (e.g. elements, faces, edges, nodes) and other entities corresponding to another instance of grid derived from the former by refinement or, vice versa, from which the former is derived. In our case, the uniform refinement procedure to be applied to an instance `gridFE` of hierarchic class `GridFeHier` is simply called by

```
gridFE.refineUniformly(&newgridFE, iMethod);,
```

while the adaptive procedure is called by

```
gridFE.refine(&newgridFE, vecMarkedElms);.
```

In both the refinement procedures the new mesh is `newgridFE`, generated from the original mesh `gridFE`. In the uniform procedure, the parameter `iMethod` is an identifier that specifies which subdivision technique has to be considered inside a list of various refinement methods implemented for 2D and 3D meshes. In the adaptive refinement routine, the information about which elements refine, and how much each one, is contained in the vector `vecMarkedElms`. Such vector associates to each global number of element in `gridFE` the number of edges that have to be split, according to the technique described in Section 5.3.

A class `GridSurfaceTriangulation` is also considered to connect mesh information with the geometry, i.e. the NURBS curves and surfaces representing boundaries and interfaces of the model. Once established such connection, any refinement procedure will be performed in accordance with the curved shape of boundaries and interfaces, by projections of the nodes located on the boundary/interface edges or faces onto such curves/surfaces (as shown previously, in Figure 6).

To conclude with mesh information, a class `NeighborFE` is defined, containing information about adjacencies of entities in the mesh, i.e. which are the elements having a node in common, the elements adjacent to an element or the nodes adjacent to a node. Finally, a class `FEcomp` allows geometric operations on elements, triangles and tetrahedra, like computation of lengths, areas, volumes, normals, barycenters, etc.

Classes for elements.

The elements can be seen as instances of a class `Element(nVertices,nBasisFunctions)`, where `nNodes` and `nBasisFunctions` represent the number of vertices (3 for triangles, 4 for tetrahedra) and the number of basis functions (3 or 6 for linear or quadratic triangles, 4 or 10 for linear or quadratic tetrahedra, and so on), respectively. The definition of the basis functions and the calculation of their first derivative (as required for the weak form of second order differential problems) can be implemented as useful member functions defining the nature of derived classes, like `ElementTetLin` from `Element(4,4)`, `ElementTetQuad` from `Element(4,10)`, and analogously for triangles, or for higher order finite element methods.

During the loop over all elements in the global finite element assembly, the current index `iElm` of element has first to be associated to an `Element` template, and successively it is geometrically located in its space position by means of a mapping from the reference element, described by the following code:

```
elm.update(iElm, grid);
mapper.mapIsoparametric(quad, elm);.
```

Here `mapper` is an instance of the class `Mapper` that performs the coordinate transformation from the reference element onto the current element. The type of Gaussian integration is specified by an instance `quad` of the class `GaussQuadrature`.

Some more independent classes can be considered for further information. For instance, `NurbsCurve` and `NurbsSurface` can be designed to perform geometric operations on curves and surfaces defined by NURBS parametric representation, while a class `Sparse` is used to handle matrices having a sparse structure.

In the next Chapter, we finally conclude our discussion with the analysis of numerical results obtained on some magnetostatic cases.

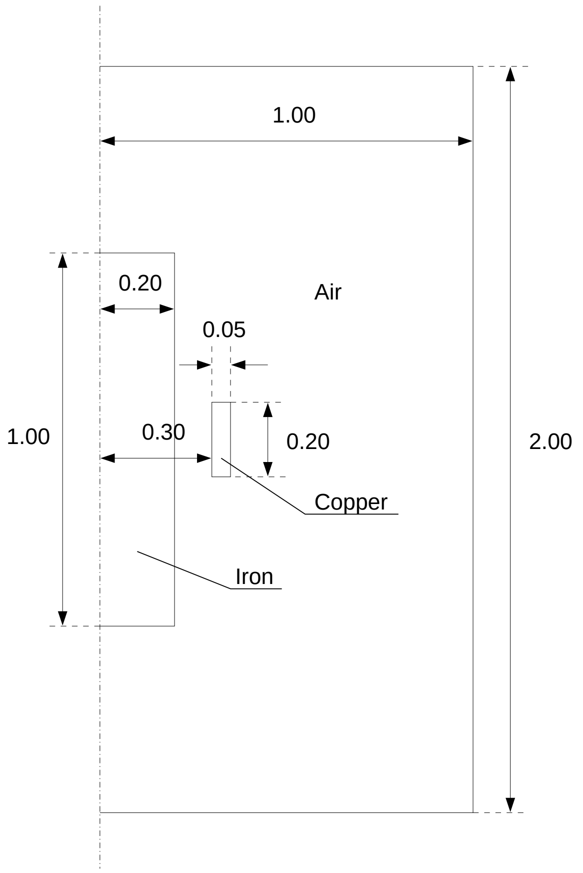

Figure 7: Axial section of the domain in Problem 1 (dimensions in meters)

7 Applications and numerical examples

7.1 Problem 1

The first problem is an axisymmetric model that describe a typical electromagnet. The model consists of three material domains. A cylindrical core of ferromagnetic material (e.g. iron) is inserted in a toroidal copper winding with azimuthal width 2π and rectangular cross section. The ferromagnetic medium and the coil are immersed in a cylindrical box containing air with perfectly conducting surfaces. Geometry and dimensions of the materials are described in Figure 7.

As data for the problem, we assign the relative magnetic permeabilities $\mu_{r,fe} = 10^4$, $\mu_{r,coil} = \mu_{r,air} = 1$ for ferromagnetic material, coil and air, respectively. A constant stationary current flows in the coil with density magnitude $J_s = 100\,A/m^2$, i.e. total intensity $1\,A$.

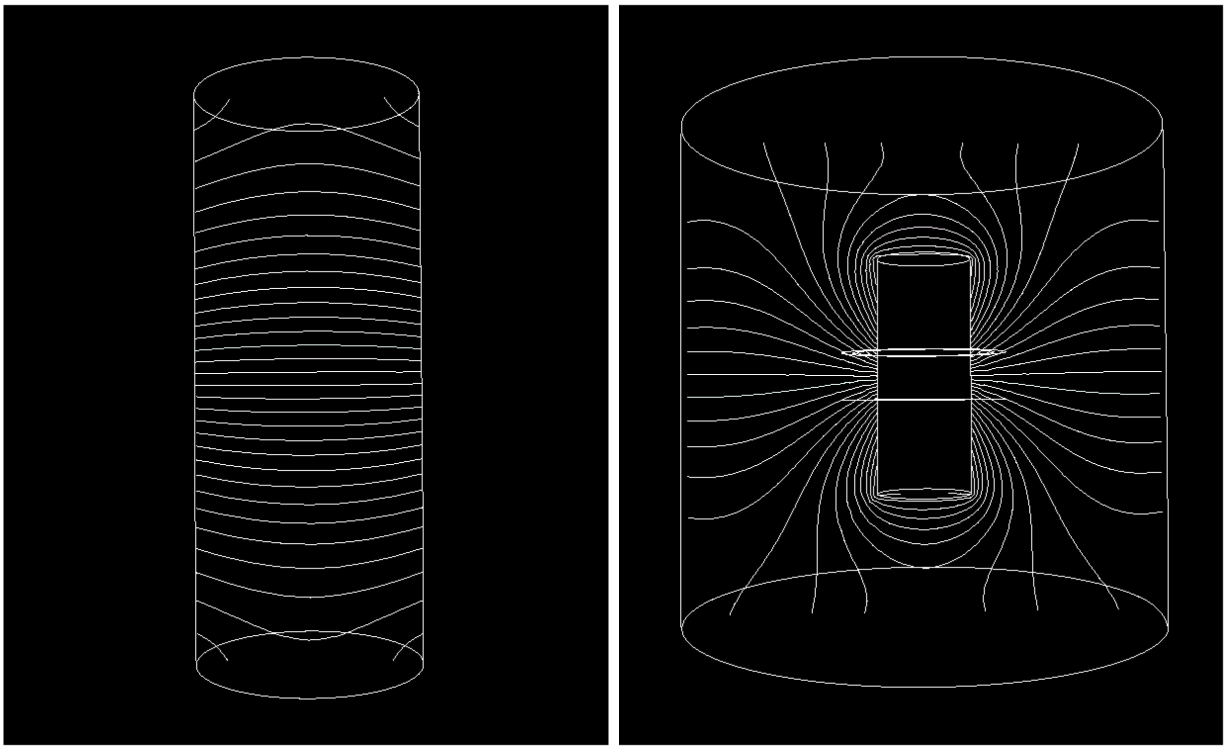

Figure 8: Isopotential lines in the total and reduced domains of Problem 1

In our double potential definition, the scalar potential is assumed to be total inside the iron core, which is simply connected, and reduced in air and inside the coil. Since the magnetic permeability is much higher inside iron, the potential has been defined total on its boundary (interface for the model). A Neumann condition has been imposed on the outer boundary, specifying a value of potential at one point in order to guarantee the uniqueness of solution.

The line integral computations have been performed by considering, point by point, the average of estimates over trees generated by initial points located in symmetric positions and sufficiently distant from each others. Since here the ferromagnetic medium has a simple convex shape, the integration lines can be simply approximated by polygonals composed of element edges lying on the interface and the boundary (if Dirichlet conditions are specified). Over each edge a 1-point quadrature rule can be applied. As expected, the mesh quality has affected the precision of the line integral computations, becoming the more accurate as the triangulation becomes finer, since by mesh refinement polygonals converge towards curves of the interface and the (possible) Dirichlet boundary. For a further improvement in the accuracy of line integral computations, also higher order methods have been considered, e.g. a composite one-dimensional Gauss-Legendre quadrature on

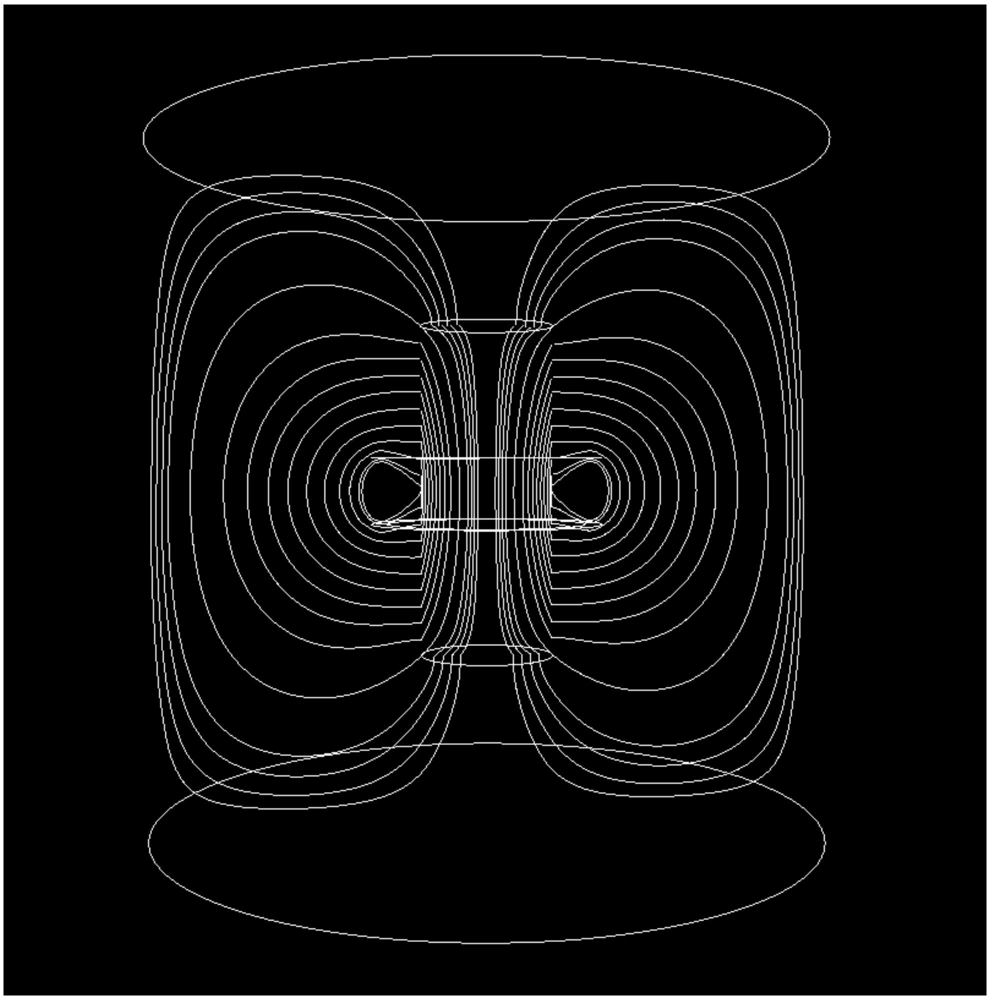

Figure 9: Magnetic field streamlines in Problem 1

each edge, by using 2-4-6 Gaussian points/weights. Tests have been completed by considering arcs instead of segments, through projection of edges onto the curved surfaces of the interface and the possible Dirichlet boundary.

Figure 8 shows the isopotential section lines along any plane containing the symmetry axis, respectively for the total and the reduced potential. Figure 9 shows the streamlines of the magnetic field intensity **H**. Notice the tangential discontinuity of the field streamlines at the interface between ferromagnetic material and air, due to magnetization effects. Most of the magnetic flux is concentrated around the ferromagnetic medium, while the flux density in air is found to be very low.

Table 1 reports the estimated values of the magnetic energy on air, iron, coil and global domain, according to definition (4.21). Values are given in comparison with the energy

FEM	Reference *2D axisym.*	LS *field* **B**	$\mathcal{LL}^*$ *dual vector* **U**	G. Edge *potential* **A**	G. Nodal *potentials* ϕ-φ
Elms	–	505 710	970 767	895 106	728 338
W_{air}	$9.089{\cdot}10^{-7}$	$8.967{\cdot}10^{-7}$	$8.947{\cdot}10^{-7}$	$9.027{\cdot}10^{-7}$	$9.100{\cdot}10^{-7}$
W_{fe}	$4.731{\cdot}10^{-10}$	$4.885{\cdot}10^{-10}$	$4.537{\cdot}10^{-10}$	$4.681{\cdot}10^{-10}$	$4.766{\cdot}10^{-10}$
W_{cu}	$3.614{\cdot}10^{-8}$	$3.333{\cdot}10^{-8}$	$3.494{\cdot}10^{-8}$	$3.575{\cdot}10^{-8}$	$3.578{\cdot}10^{-8}$
W_{tot}	$9.455{\cdot}10^{-7}$	$9.305{\cdot}10^{-7}$	$9.301{\cdot}10^{-7}$	$9.389{\cdot}10^{-7}$	$9.462{\cdot}10^{-7}$

Table 1: Values of magnetic energies in Problem 1 (in Joule)

estimates computed by other FEM techniques, by considering in all cases a piecewise linear discretization. Our results, by adaptive Galerkin finite element solution in terms of potentials $\phi - \varphi$, appear in the last column. The values here reported have been obtained by choosing $\delta_S = \delta_N = 0.5$ as refinement factors on the coil and the air/iron region (called, for brevity, *non-source* region) respectively.

As regards the other techniques, column 1 of Table 1 reports the reference values provided by ABB Corporate Research, from solution of the equivalent 2D problem due to axial symmetry, while values reported in columns 2, 3 and 4 are computed respectively by using methods (a), (b) and (c), described in the following:

(a) least-squares finite element solution by field formulation in terms of vector **B** [8, 9];

(b) finite element solution via the $\mathcal{LL}^*$ method, i.e. by a "dual" formulation in term of a vector **U**, such that $\mathbf{B} = \mathcal{M}\mathcal{L}^*\mathbf{U}$, for a symmetric positive definite bounded operator $\mathcal{M}$ and an adjoint operator $\mathcal{L}^*$ associated to the field equations [10];

(c) Galerkin finite element solution by potential formulation in terms of vector **A**, using edge elements [9].

Methods (a) and (c) are classical finite element approaches well-known from the literature, while method (b) is a more recent technique, whose application to static Maxwell's equations is currently being studied by M.G. Larson, K. Samuelsson and R. Bergström at Chalmers Finite Element Center. These methods have been accompanied by adaptive techniques of mesh refinement, with criteria based on estimation of suitable residual quantities or error bounds (see details in Chapter 2 of [9], and Chapter 3 of [10]). Among them, we point out the a posteriori error estimation in the adaptive $\mathcal{LL}^*$ method, based on a derivation of proper upper bounds for the finite element error of **U** in energy norm, by means of interior residuals and inter-element fluxes. Similarly to our approach, a formal argument of elementwise decomposition has been used, here for a different formulation.

Values confirm the better convergence, for the same order of polynomial approximation, of the Galerkin solution in our double potential formulation with respect to a solution by the least-squares method, or the $\mathcal{LL}^*$ method. In this model having a simple geometry,

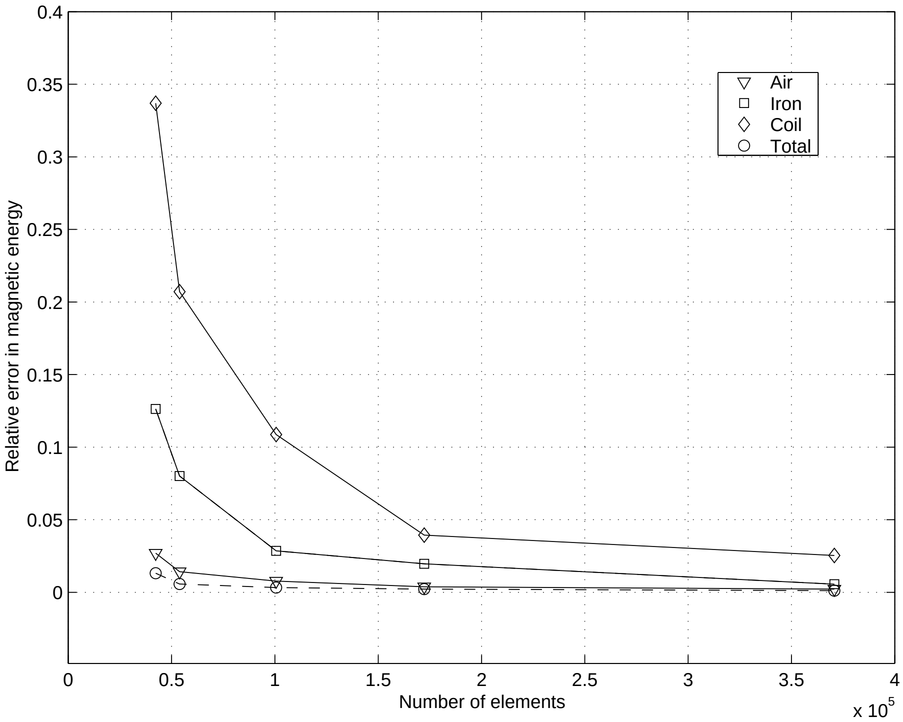

Figure 10: Convergence of the magnetic energy in Problem 1 (adaptive refinement)

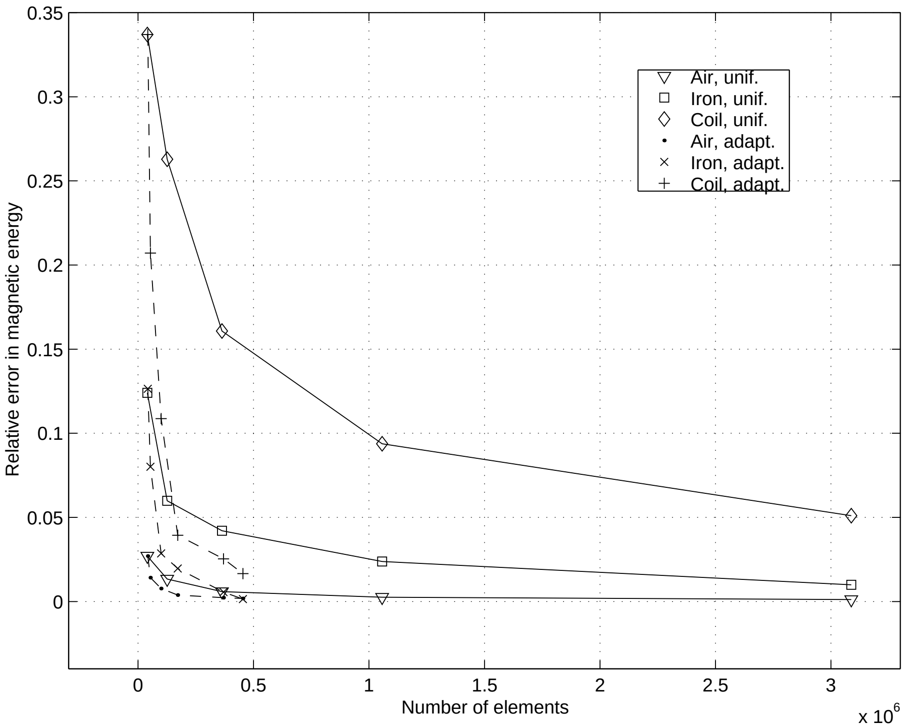

Figure 11: Convergence of the magnetic energy in Problem 1 (uniform vs. adaptive refinement)

N. nodes	N. elms	W_{air}	W_{iron}	W_{coil}	W_{tot}
8115	42346	0.0270	0.1264	0.3369	0.0132
10296	53875	0.0142	0.0801	0.2071	0.0058
18715	100579	0.0077	0.0286	0.1087	0.0033
31667	172247	0.0039	0.0196	0.0394	0.0022
67351	370707	0.0022	0.0056	0.0254	0.0012
82544	454421	0.0018	0.0015	0.0166	0.0011

Table 2: Values of relative errors in magnetic energy (cfr. Figure 10)

values result even slightly better than the ones obtained from a Galerkin solution of the problem in vector potential formulation using linear edge elements. Besides, a fair accuracy in our method is reached at a sufficiently low number of degrees of freedom. As an example, if we choose refinement factors $\delta_S = 0.3$ and $\delta_N = 0.5$ in source and non-source regions, respectively, the following magnetic energy values are obtained: $W_{air} = 9.107 \cdot 10^{-7}\ J$, $W_{fe} = 4.790 \cdot 10^{-10}\ J$, $W_{cu} = 3.561 \cdot 10^{-8}\ J$, with a total energy $W_{tot} = 9.467 \cdot 10^{-7}\ J$, corresponding to a mesh composed of 75179 nodes and 415849 elements.

Figure 10 describes the behaviour of the relative error in the magnetic energies, strongly decreasing as the number of elements increases, using the technique of adaptive mesh refinement described in Chapter 5. The corresponding error values are reported in Table 2. Here, refinement factors $\delta_S = \delta_N = 0.6$ have been considered in both source and non-source regions. Figure 11 shows the slower decrease of relative errors when an uniform refinement is applied, instead of our adaptive scheme, with superposition in scale of the corresponding relative error curves estimated by adaptive refinement. The convergence of the solution is accompanied by a monotonic decrease of the relative a posteriori error (5.40) at each successive refinement iteration.

The adaptive refinement procedure, when applied, leads to a stronger refinement near the interface, especially close to the corners of the ferromagnetic medium, as it is evident from Figure 12, which shows a detail of the initial and the refined mesh at the top of iron. The second mesh of Figure 12 has been obtained after 4 refinement iterations, considering the same refinement factors corresponding to the error trend depicted in Figure 10.

Results show that the convergence in the current-carrying conductor is slower than the one in air or inside the ferromagnetic core. This is due to a contribution of the modelling error, owing to the computation method of the Biot-Savart law. Such error contribution has been proved to be larger in regions inside or near the conductor. See in [27] how the particular choice of the integration method of the Biot-Savart law can affect accuracy and computational time in the evaluation of $\mathbf{H}_s$ and, therefore, of the magnetic energy values. The data reported here have been computed by resorting to Urankar's semi-analytical

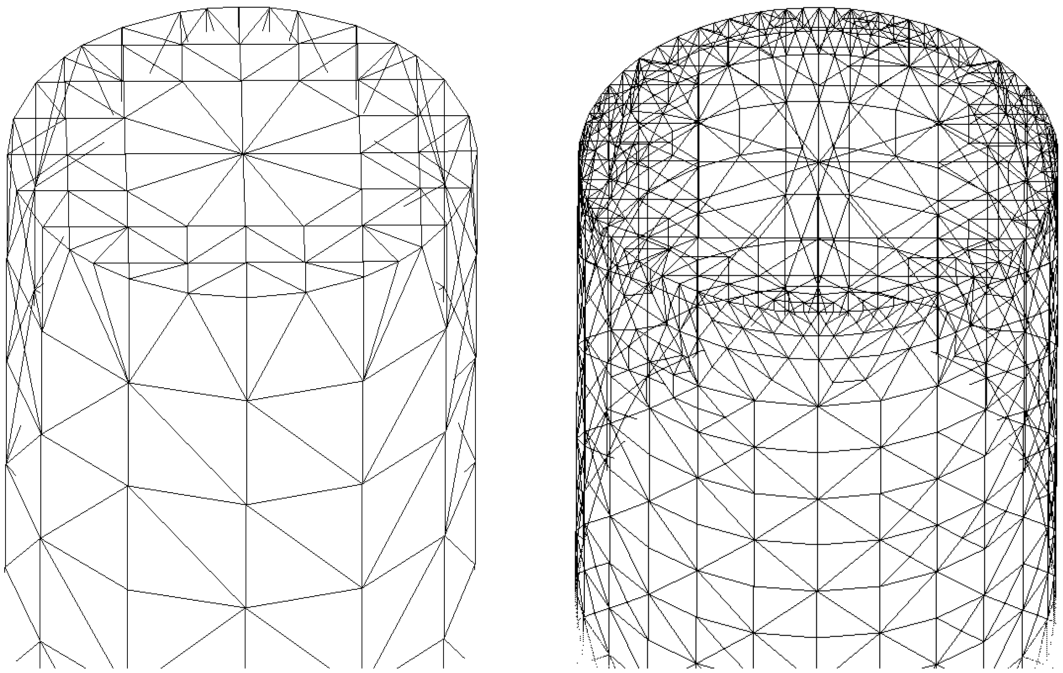

Figure 12: Detail of initial and adaptively refined mesh at the interface (Problem 1)

method, as its results are (especially close to the coil) generally more accurate than a finite volume integration and, above all, particularly fast. Concerning finite volume integration techniques, test have been done by considering a composite Gauss-Legendre quadrature, applied to each tetrahedron inside the coil, choosing 1-4-12 point rules on each element. In this case, it has been observed that accuracy is more sensitive to the size of integration volumes than to the quadrature order applied to each volume.

7.2 Problem 2

The second problem is an axisymmetric model, as in the previous case, but a more complex, non-convex geometry is provided. The material configuration consists of a ferromagnetic medium having a typical revolved C-shape whose central trunk is surrounded by the same toroidal copper coil as in Problem 1, immersed in the same cylindrical box of air having perfectly conducting boundaries. Geometry and dimensions are described in Figure 13.

The problem has been solved by considering two different ratios between the diffusive

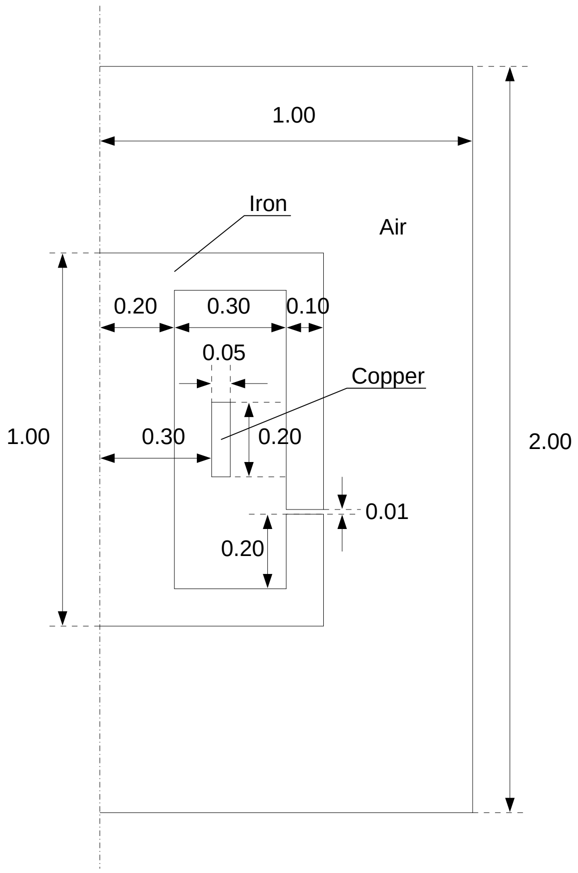

Figure 13: Axial section of the domain in Problem 2 (dimensions in meters)

coefficients. For the ferromagnetic medium, it has been assumed $\mu_{r,fe} = 100$ or $\mu_{r,fe} = 10^4$ and, for coil and air, $\mu_{r,coil} = \mu_{r,air} = 1$. Again, we consider a stationary current with constant density magnitude $J_s = 100\,A/m^2$.

Figure 14 shows the field streamlines in the case $\mu_{r,fe} = 100$. This configuration, like all C-shaped geometries, is characterized by a significant potential difference in the air gap, i.e. the channel separating ferromagnetic components, the higher it is the thinner the gap is, and the higher the ferromagnetic permeability is. Notice in Figure 14 the curvature inflection of the field streamlines in the air region between the coil and the gap of the ferromagnetic medium.

In this case, due to the non-convex geometry of the ferromagnetic domain, equipped with corners and edges, a particular care is required in the computation of the line integrals defining the jumps between potentials at the interface, or values of a possible Dirichlet boundary condition. A possible way to increase the accuracy of such line integral computations is too avoid “too long” trees, as it would occur in this case. Aiming at this, a

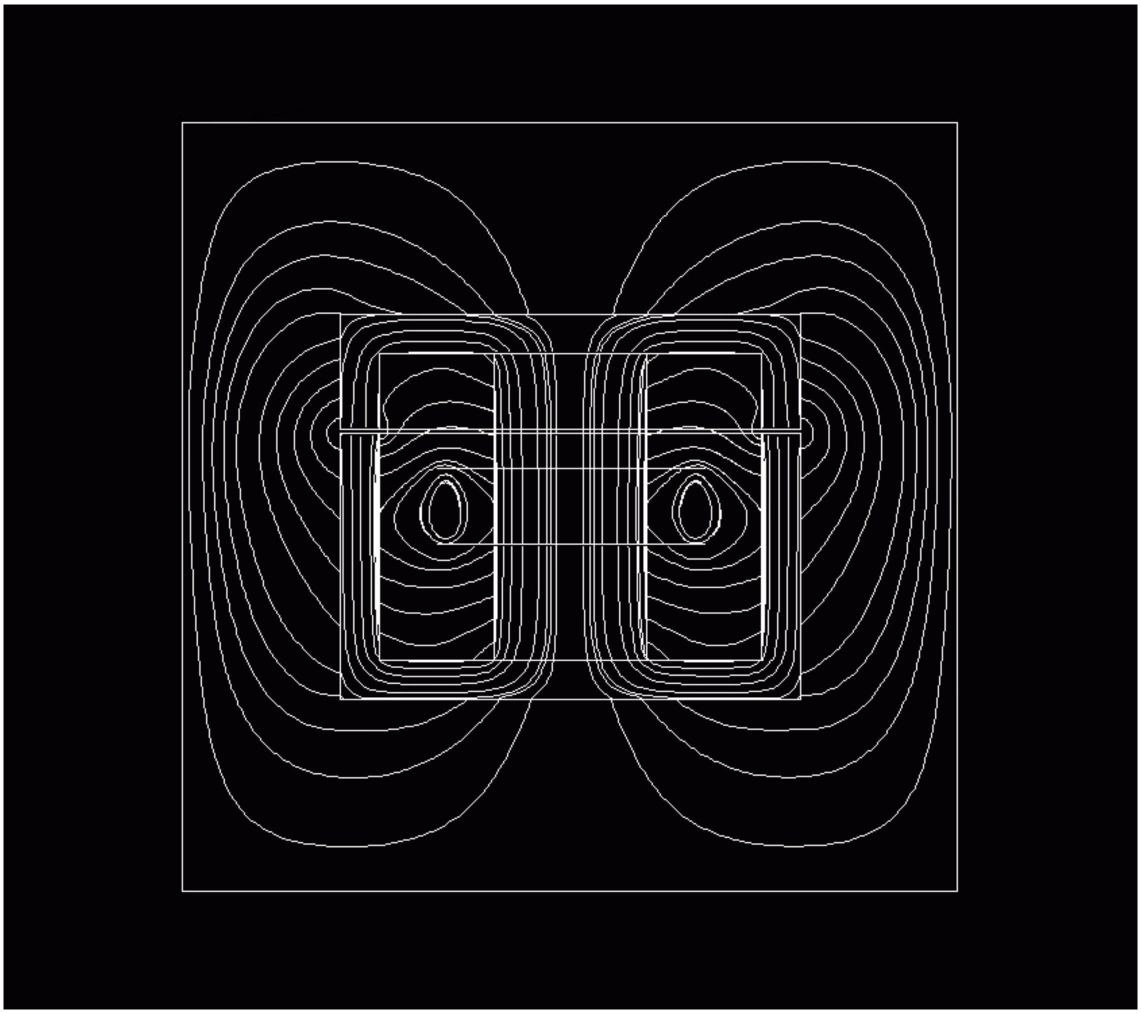

Figure 14: Magnetic field streamlines in Problem 2 (case $\mu_{r,fe} = 100$)

partition of the interface in several surface regions has been considered. Thus, line integrals have been computed on each part, with estimation of their values along paths connecting a starting point in one region with another in a successive region. Finally, partial trees on single regions have been assembled into global trees covering the overall interface, node by node. Similar procedures are suggested for complex-shaped models, as they are frequently encountered in real electromagnetic devices. As in Problem 1, integration lines are polygonals along planes, or unions of elementary arcs by edge projection along curved surfaces. Then, a numerical integration has been performed over each segment/arc by using a 2-4-6 point linear/curvilinear Gauss-Legendre quadrature.

Tables 3 and 4 report estimates of the magnetic energies in air, ferromagnetic medium, coil and global domain, in the two cases $\mu_{r,fe} = 100$ and $\mu_{r,fe} = 10^4$ respectively. Results

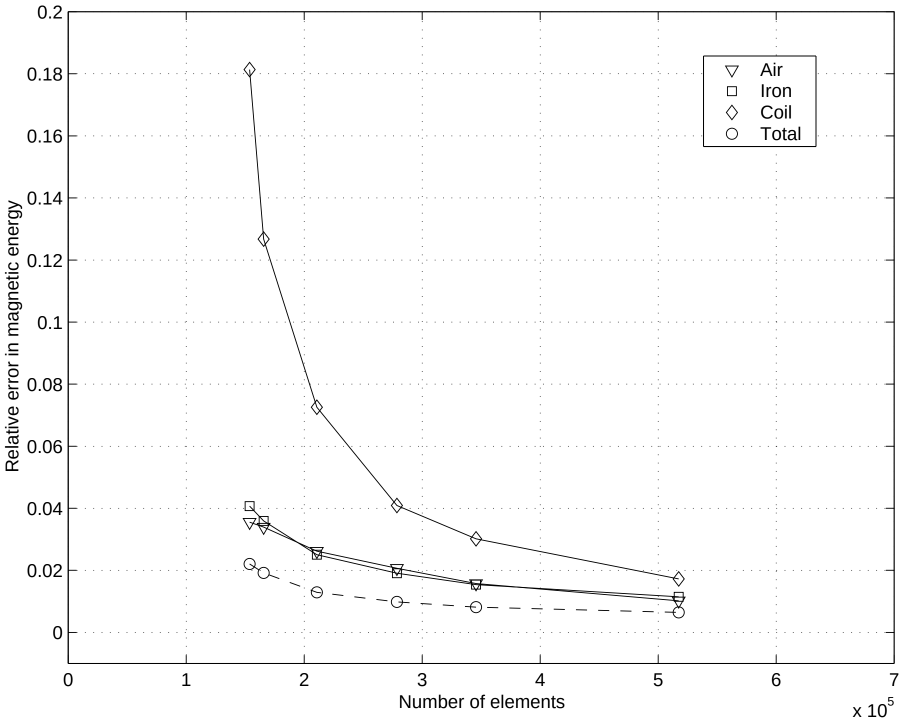

Figure 15: Convergence of the magnetic energy in Problem 2 (case $\mu_{r,fe} = 100$)

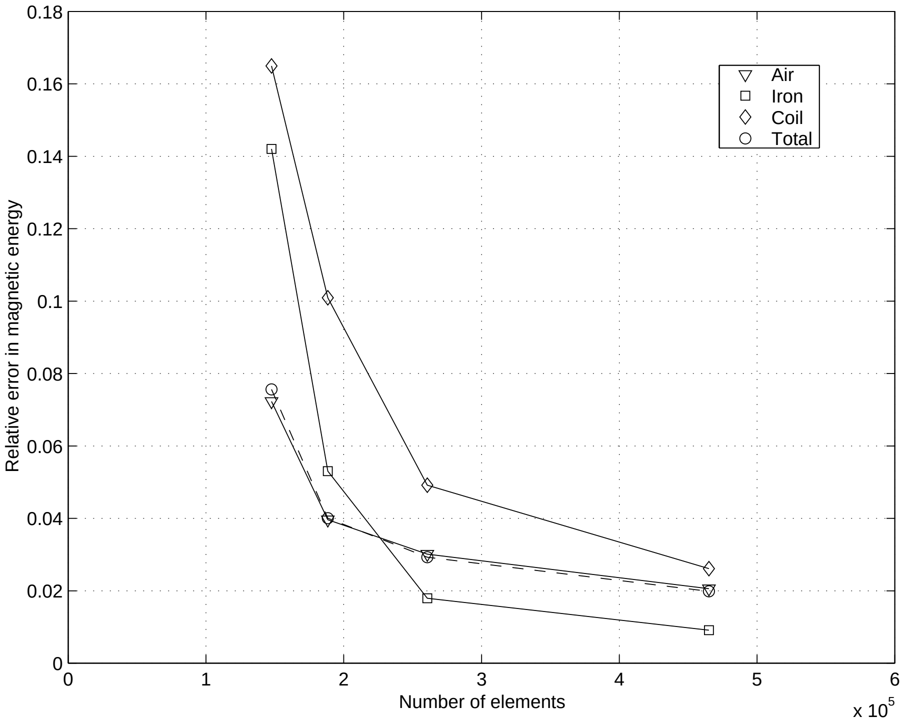

Figure 16: Convergence of the magnetic energy in Problem 2 (case $\mu_{r,fe} = 10^4$)

FEM	Reference *2D axisym.*	G. Edge *potential* **A**	G. Nodal *potential* **A**	G. Nodal *potentials* $\phi - \varphi$
Elms	–	819 922	959 231	810 662
W_{air}	$1.025 \cdot 10^{-6}$	$1.025 \cdot 10^{-6}$	$1.114 \cdot 10^{-6}$	$1.019 \cdot 10^{-6}$
W_{fe}	$3.564 \cdot 10^{-6}$	$3.517 \cdot 10^{-6}$	$2.785 \cdot 10^{-6}$	$3.591 \cdot 10^{-6}$
W_{cu}	$3.596 \cdot 10^{-8}$	$3.529 \cdot 10^{-8}$	$4.079 \cdot 10^{-8}$	$3.564 \cdot 10^{-8}$
W_{tot}	$4.625 \cdot 10^{-6}$	$4.577 \cdot 10^{-6}$	$3.940 \cdot 10^{-6}$	$4.646 \cdot 10^{-6}$

Table 3: Values of magnetic energies in Problem 2 (case $\mu_{r,fe} = 100$)

FEM	Reference *2D axisym.*	G. Edge *potential* **A**	G. Nodal *potential* **A**	G. Nodal *potentials* $\phi - \varphi$
Elms	–	536 963	189 887 (Q)	527 046
W_{air}	$2.609 \cdot 10^{-5}$	$2.558 \cdot 10^{-5}$	$2.645 \cdot 10^{-5}$	$2.655 \cdot 10^{-5}$
W_{fe}	$1.524 \cdot 10^{-6}$	$1.525 \cdot 10^{-6}$	$1.270 \cdot 10^{-6}$	$1.506 \cdot 10^{-6}$
W_{cu}	$6.500 \cdot 10^{-8}$	$6.361 \cdot 10^{-8}$	$6.522 \cdot 10^{-8}$	$6.367 \cdot 10^{-8}$
W_{tot}	$2.768 \cdot 10^{-5}$	$2.717 \cdot 10^{-5}$	$2.779 \cdot 10^{-5}$	$2.812 \cdot 10^{-5}$

Table 4: Values of magnetic energies in Problem 2 (case $\mu_{r,fe} = 10^4$)

obtained by our $\phi - \varphi$ formulation are described in the last column. The values that appear in the first table have been computed by choosing $\delta_S = 0.5$ and $\delta_N = 0.65$ as refinement factors in the source and non-source regions, while factors $\delta_S = 0.5$ and $\delta_N = 0.71$ have been considered in the second table. Again, results are given in comparison with energy estimates computed by other finite element techniques. First, column 1 reports the reference values from ABB Corporate Research. Columns 2 reports results obtained from an adaptive Galerkin finite element solution in vector potential formulation, using linear edge elements. An adaptive Galerkin solution has been used also to estimate values in column 3, still in vector potential formulation, but in this case nodal elements have been used, linear in case $\mu_{r,fe} = 100$, and quadratic in case $\mu_{r,fe} = 10^4$.

Details about results obtained from the vector potential formulation via edge and nodal elements, together with further tables, are reported in [9]. Differently from Table 1 for Problem 1, values obtained from least-squares finite element solution are not reported here, since they do not result enough accurate for this complex-shaped geometry, even when considering quadratic elements. The $\mathcal{LL}^*$ method is currently under investigation for this type of non-convex configuration, and results are not yet available. When a high ferromagnetic permeability is considered, e.g. $\mu_{r,fe} = 10^4$, at least a quadratic approximation is required in a vector potential formulation solved by nodal elements, to reach a fair accuracy. As concerns our double scalar potential formulation, even in this case results confirm a good accuracy, comparable to the one reached by edge elements, well-known to be particularly efficient for vector formulations.

Figures 15 and 16 depict the decreasing trend of the relative error in the magnetic energies for an increasing number of elements when mesh refinement occurs in adaptive way. In Figure 15, refinement factors $\delta_S = 0.7$ and $\delta_N = 0.8$ have been considered in the source and non-source regions, while in Figure 16 respectively factors $\delta_S = 0.5$ and $\delta_N = 0.725$ have been used. Notice that in these examples a sharper refinement has been required inside the source conductor. Although a small refinement factor δ_S has the relative error decreased very fastly inside the source region, we observe in all cases a lower accuracy of error values inside the coil with respect to values in air and inside the ferromagnetic material, owing to the above mentioned modelling error in the computation of the Biot-Savart law.

8 Conclusions and future work

An adaptive finite element solution of a class of three-dimensional magnetostatic problems has been proposed, obtained from a scalar potential $\phi - \varphi$ formulation of static Maxwell's equations. The resulting boundary value problem is a generalized Poisson model with mixed non-homogeneous boundary and interface conditions of Dirichlet and Neumann type. The finite element discretization consists of a piecewise linear Galerkin method on tetrahedral mesh (Chapter 4). A posteriori estimates of the finite element error have been proved in energy norm, to provide criteria for an adaptive strategy of h-refinement of the mesh (Chapter 5).

Results (Chapter 7) on test cases and comparisons with other finite element techniques, show an higher accuracy of our adaptive finite element solution via $\phi - \varphi$ formulation, with respect to adaptive finite element methods based on formulations by fields (e.g. least-squares techniques) or dual vectors (e.g. the $\mathcal{L}\mathcal{L}^*$ method), for the same order of polynomial approximation. Besides, our adaptive scheme produces more accurate results than an adaptive Galerkin solution via vector potential formulation using *nodal* elements, for the same order. Finally, the quality of results is comparable to the one resulting from an adaptive Galerkin solution in vector potential formulation when *edge* elements are considered, for the same order, these latter being well-known for their efficiency in finite element vector solutions.

A fundamental modelling aspect is the estimation of the magnetic field due to imposed currents, by computation of the Biot-Savart law whose accuracy affects particularly the final accuracy in results. For coil geometries, the Biot-Savart law has been computed resorting to Urankar's semi-analytical method, with estimation of elliptic integrals. For complex-shaped current-carrying regions, a finite volume integration has been considered, consisting of a composite Gauss-Legendre quadrature over all elements inside the source conductors. Besides, the accuracy of results is also influenced by the accuracy of the numerical integration scheme used for computing line integrals defining values of Dirichlet boundary conditions or jumps of discontinuity at the interface between potentials, due to the source magnetic field.

The several aspects of modelling and computation involved in the present work suggest many tasks for future work. Concerning computation, higher order Galerkin finite element methods should be considered. Multigrid tecniques could be applied as preconditioners for the finite element solution, by using the hierarchy of nested refined grids. Concerning a posteriori error analysis, since estimates here have been defined for the error of the finite element solution, i.e. at potential level, it appears interesting as a successive stage to measure the error associated to the energy norm of the potential, since it is related to the magnetic energy. Besides, for a more complete error analysis, estimates for the modelling error should be considered, mainly the error due to the computation of the Biot-Savart law and the estimation of line integrals on Dirichlet surfaces. Such modelling error contributions could be taken into account, together with the a posteriori finite element error, for a modified strategy of mesh refinement, aiming at an improvement of results especially in regions close to coil.

Finally, for an analysis of a complete magnetostatic case, a generalization of our model should be considered with introduction of permanent magnets, so that the contribution of the coercive field $\mathbf{H}_c$ is also taken into account.

Acknowledgements

I wish to thank particularly Prof. Claes Johnson for his affable hospitality at Chalmers Finite Element Center of Chalmers University of Technology in Göteborg, Sweden. I wish to express to him my deep and sincere gratitude for his scientific and moral support, for some precious remarks after reading my report and for brilliant, inspiring conversations.

I am grateful to all the people of the center and the Department of Mathematics of Chalmers University and Göteborg University, contributing - with help, teaching, resources and kindness - to a very pleasant working environment. Among them, I express my gratitude particularly to Klas Samuelsson, for his precious teaching and help in questions dealing with C++ code, for fruitful dicussions on some numerical aspects, and for his advice after reading my report. I owe gratitude to Rickard Bergström and Niklas Ericsson, for their help and patience in answering all the times my questions about C++ code and Unix systems, and for the many books they lent me.

Concerning the finite element software performed in this research project, I wish to thank Klas for his code about the grid classes, together with Rickard whose code has been used by me as an initial basis for implementation.

Finally, I am also grateful to Alessandro Castagnini of ABB Ricerca in Milano, Italy, Piergiorgio Alotto of the Department of Electrical Engineering in Genova University, Italy, Andrea Bertoni of TechnoSoft s.a.s. in Genova, and Paolo Fernandes of the Istituto per la Matematica Applicata IMA-CNR in Genova, for their help, their suggestions, and for the initial inspiration about the subject of the present work.

This work has been financially supported by the National Research Council (CNR) of Italy, through research fellowships, grant n. 203.01.70 for Mathematical Sciences.

References

[1] M. Abramowitz, I.A. Stegun, *Handbook of Mathematical Functions*, Dover Publications, New York (1968)

[2] P. Alotto, A. Castagnini, P. Girdinio, P. Fernandes, *Error estimation and adaptive meshing in 3D electrostatic and magnetostatic problems*, IEEE Trans. Magn. 34, 3260-3263 (1998)

[3] I. Babuska, W.C. Reimbholdt, *A posteriori error estimates for the finite element method*, Int. J. Num. Meth. Eng. 12, 1597-1615 (1978)

[4] S. Balay, W.D. Gropp, L.C. McInnes, B.F. Smith, *PETSc 2.0 Users Manual*, Technical report ANL-95/11 - Revision 2.0.28, Argonne National Laboratory (2000)

[5] R.E. Bank, A. Weiser, *Some a posteriori error estimators for elliptic partial differential equations*, Math. Comput. 44, 283-301 (1985)

[6] J.J. Barton, L.R. Nackman, *Scientific and engineering C++*, Addison-Wesley (1997)

[7] R. Becker, R. Rannacher, *A feed-back approach to error control in finite element methods: basic analysis and examples*, East-West J. Num. Math 4, 237-264 (1996)

[8] R. Bergström, *Least-squares finite element methods for electromagnetic applications*, Lic. Thesis, Dept. Mathematics, Chalmers University of Technology, Göteborg (2000)

[9] R. Bergström, A. Bondeson, C. Johnson, M.G. Larson, Y. Liu, K. Samuelsson, *Adaptive finite element methods in electromagnetics*, Technical report 2, ITM - Swedish Institute of Applied Mathematics (1999)

[10] R. Bergström, M. Larson, K. Samuelsson, *The $\mathcal{LL}^*$ finite element method and multigrid for the magnetostatic problem*, Chalmers Finite Element Center Preprint 2001-02, Chalmers University of Technology, Göteborg (2001)

[11] M. Bern, D. Eppstein, *Mesh generation and optimal triangulation*, in *Computing in Euclidean Geometry*, D.Z. Du, F. Hwang eds., World Scientific, 23-90 (1992)

[12] P.F. Byrd, M.D. Friedman, *Handbook of Elliptic Integrals for Engineers and Scientists*, Springer, New York (1971)

[13] X. Cai, K. Samuelsson, *Parallel multilevel methods with adaptivity on unstructured grids*, Comput. Visual. Sci. 3, 133-146 (2000)

[14] B.C. Carlson, *Computing elliptic integrals by duplication*, Num. Math. 33, 1-16 (1979)

[15] A. Castagnini, *Error estimation and mesh adaption techniques for 3D finite element methods*, Ph.D. Thesis, Dip. Ingegneria Elettrica, Universita' degli Studi di Genova (1998)

[16] D.K. Cheng, *Field and Wave Electromagnetics*, Addison-Wesley (1983)

[17] P.G. Ciarlet, *The Finite Element Method for Elliptic Problems*, North Holland, Amsterdam (1978)

[18] K. Eriksson, D. Estep, P. Hansbo, C. Johnson, *Introduction to adaptive methods for differential equations*, Acta-Numerica 4, 105-158 (1995)

[19] K. Eriksson, D. Estep, P. Hansbo, C. Johnson, *Computational Differential Equations*, Cambridge University Press (1996)

[20] K. Eriksson, C. Johnson, *An adaptive finite element method for linear elliptic problems*, Math. Comput. 50, 361-383 (1988)

[21] K. Eriksson, C. Johnson, *Adaptive finite element methods for parabolic problems I: A linear model problem*, SIAM J. Num. An. 28, 43-77 (1991)

[22] L.C. Evans, *Partial Differential Equations*, in *Graduate Studies in Mathematics*, Vol. 19, American Mathematical Society Providence Rhode Island (1998)

[23] P. Fernandes, M. Fontana, *Adaptive finite element analysis of a 2D time dependent eddy current problem, Part I: Finite element model and local error estimation*, IMA Report 2, Consiglio Nazionale delle Ricerche, Italy (1998)

[24] P. Fernandes, P. Girdinio, *Adaptive finite element analysis of 2D static and steady state electromagnetic problems*, Int. J. Num. Meth. Eng. 45, 215-243 (1999)

[25] P. Fernandes, P. Girdinio, G. Molinari, *Techniques of h-refinement in adaptive meshing algorithms*, COMPEL - Int. J. Comp. Math. Electric Electronic Eng. 13, 329-334 (1994)

[26] M. Fontana, *Experience and ideas on adaptive finite element methods at Chalmers Finite Element Center*, Technical Note, Chalmers Finite Element Center, Chalmers University of Technology, Göteborg (1999)

[27] M. Fontana, *Integration methods for the calculation of the magnetostatic field due to coils*, Chalmers Finite Element Center Preprint 2001-07, Chalmers University of Technology, Göteborg (2001)

[28] W.H. Hayt, *Engineering Electromagnetics*, McGraw-Hill (1987)

[29] J. Jin, *The Finite Element Method in Electromagnetics*, J. Wiley and Sons (1993)

[30] C. Johnson, *Numerical Solution of Partial Differential Equations by the Finite Element Method*, Studentlitteratur (1987)

[31] C. Johnson, *Adaptive finite element methods for diffusion and convection problems*, Comp. Meth. App. Mech. Eng. 82, 301-322 (1990)

[32] D.W. Kelly, J.P. de S.R. Gago, O.C. Zienkiewicz, *A posteriori error analysis and adaptive processes in the finite element method: Part I - Error analysis*, Int. J. Num. Meth. Eng. 19, 1593-1619 (1983)

[33] D.W. Kelly, J.P. de S.R. Gago, O.C. Zienkiewicz, *A posteriori error analysis and adaptive processes in the finite element method: Part II - Adaptive mesh refinements*, Int. J. Num. Meth. Eng. 19, 1621-1656 (1983)

[34] M. Krizek, P. Neittaanmäki, *Mathematical and Numerical Modelling in Electrical Engineering*, Kluwer Academic Publishers (1996)

[35] E.H. Neville, *Jacobian Elliptic Functions*, Oxford Clarendon Press (1951)

[36] W.H. Press, S.A. Teukolsky, W.T. Vetterling, B.P. Flannery, *Numerical recipes in C*, Cambridge University Press (1992)

[37] A. Quarteroni, A. Valli, *Numerical approximation of partial differential equations*, Springer-Verlag (1994)

[38] M. Renardy, R.C. Rogers, *An Introduction to Partial Differential Equations*, Springer-Verlag (1993)

[39] M.C. Rivara, *Algorithms for refining triangular grids suitable for adaptive and multigrid techniques*, Int. J. Num. Meth. Eng. 20, 745-756 (1984)

[40] W. Rudin, *Real and complex analysis*, McGraw-Hill (1987)

[41] K. Samuelsson, *Adaptive algorithms for finite element methods approximating flow problems*, Ph.D. Thesis, Royal Institute of Technology, Stockholm (1996)

[42] P.P. Silvester, R.L. Ferrari, *Finite Elements for Electrical Engineers*, Cambridge University Press (1983)

[43] V. Thomee, S. Larsson, *Partial Differential Equations with Numerical Methods*, Chalmers University of Technology, Göteborg (1999)

[44] M. Touma Holmberg, *Three-dimensional finite element computation of eddy currents in synchronous machines*, Ph.D. Thesis, Dept. Electric Power Engineering, Chalmers University of Technology, Göteborg (1998)

[45] C.W. Trowbridge, *An Introduction to Computer Aided Electromagnetic Analysis*, J. Wiley and Sons (1992)

[46] L.U. Urankar, *Vector potential and magnetic field of current-carrying finite arc segment in analytical form. Part II: Thin sheet approximation*, IEEE Trans. Magn. 18, 911-917 (1982)

[47] L.U. Urankar, *Vector potential and magnetic field of current-carrying finite arc segment in analytical form. Part III: Exact computation for rectangular cross section*, IEEE Trans. Magn. 18, 1860-1867 (1982)

[48] L.U. Urankar, *Vector potential and magnetic field of current-carrying finite arc segment in analytical form. Part V: Polygon cross section*, IEEE Trans. Magn. 26, 1171-1180 (1990)

[49] R. Verfurth, *A review of a posteriori error estimation and adaptive mesh refinement techniques*, Wiley&Teubner (1996)

[50] O.C. Zienkiewicz, *The Finite Element Method in Engineering Science*, McGraw-Hill (1971)

Chalmers Finite Element Center Preprints

2000–01 *Adaptive Finite Element Methods for the Unsteady Maxwell's Equations*
Johan Hoffman

2000–02 *A Multi-Adaptive ODE-Solver*
Anders Logg

2000–03 *Multi-Adaptive Error Control for ODEs*
Anders Logg

2000–04 *Dynamic Computational Subgrid Modeling* (Licentiate Thesis)
Johan Hoffman

2000–05 *Least-Squares Finite Element Methods for Electromagnetic Applications* (Licentiate Thesis)
Rickard Bergström

2000–06 *Discontinuous Galerkin Methods for Incompressible and Nearly Incompressible Elasticity by Nitsche's Method*
Peter Hansbo and Mats G. Larson

2000–07 *A Discountinuous Galerkin Method for the Plate Equation*
Peter Hansbo and Mats G. Larson

2000–08 *Conservation Properties for the Continuous and Discontinuous Galerkin Methods*
Mats G. Larson and A. Jonas Niklasson

2000–09 *Discontinuous Galerkin and the Crouzeix-Raviart element: Application to elasticity*
Peter Hansbo and Mats G. Larson

2000–10 *Pointwise A Posteriori Error Analysis for an Adaptive Penalty Finite Element Method for the Obstacle Problem*
Donald A. French, Stig Larson and Ricardo H. Nochetto

2000–11 *Global and Localised A Posteriori Error Analysis in the Maximum Norm for Finite Element Approximations of a Convection-Diffusion Problem*
Mats Boman

2000–12 *A Posteriori Error Analysis in the Maximum Norm for a Penalty Finite Element Method for the Time-Dependent Obstacle Problem*
Mats Boman

2000–13 *A Posteriori Error Analysis in the Maximum Norm for Finite Element Approximations of a Time-Dependent Convection-Diffusion Problem*
Mats Boman

2001–01 *A Simple Nonconforming Bilinear Element for the Elasticity Problem*
Peter Hansbo and Mats G. Larson

2001–02 *The $\mathcal{LL}^*$ Finite Element Method and Multigrid for the Magnetostatic Problem*
Rickard Bergström, Mats G. Larson, and Klas Samuelsson

These preprints can be obtained from

`www.phi.chalmers.se/preprints`